cmgh
CELLULAR AND MOLECULAR GASTROENTEROLOGY AND HEPATOLOGY

ORIGINAL RESEARCH

Cortactin Facilitates Malignant Transformation of Dysplastic Cells in Gastric Cancer Development

Alexis A. Guenther,[1,2,*] Suyeon Ahn,[1,3,*] Jimin Min,[1,3,9,*] Changqing Zhang,[1,3] Hyuk-Joon Lee,[4,5] Han-Kwang Yang,[4,5] Bong Hwan Sung,[2,6,7] Alissa M. Weaver,[2,6,7,8] and Eunyoung Choi[1,2,3]

[1]Epithelial Biology Center, Vanderbilt University Medical Center, Nashville, Tennessee; [2]Department of Cell and Developmental Biology, Vanderbilt University School of Medicine, Nashville, Tennessee; [3]Department of Surgery, Vanderbilt University Medical Center, Nashville, Tennessee; [4]Department of Surgery, Seoul National University College of Medicine, Seoul, Korea; [5]Cancer Research Institute, Seoul National University College of Medicine, Seoul, Korea; [6]The Vanderbilt Center for Extracellular Vesicle Research, Vanderbilt University School of Medicine, Nashville, Tennessee; [7]Program in Cancer Biology, Vanderbilt University School of Medicine, Nashville, Tennessee; [8]Department of Pathology, Microbiology, and Immunology, Vanderbilt University Medical Center, Nashville, Tennessee; and [9]Current affiliation: Department of Translational Molecular Pathology, Sheikh Ahmed Center for Pancreatic Cancer Research, The University of Texas MD Anderson Cancer Center, Houston, Texas

SUMMARY

This work reveals a novel role of cortactin in the malignant transformation of dysplastic cells, thereby contributing to the understanding of undiscovered cellular mechanisms in early gastric cancer biology.

BACKGROUND & AIMS: Epithelial cancer onset occurs through sequential stages of cell lineage conversion and functional dysregulation. Dysplasia is a precancerous lesion defined as a direct precursor to cancer and is histologically defined as a transition stage between pre-cancer and cancer, but molecular and biological mechanisms controlling its transformation to malignancy are underdetermined. Here, we discover the crucial role of the actin stabilization and exosome secretion-regulatory protein cortactin in dysplastic cell transformation to adenocarcinoma.

METHODS: We engineered a CRISPR/Cas9-based cortactin knock-out (KO) dysplasia organoid model established from dysplastic tissue and examined malignant roles of cortactin during gastric cancer development *in vitro* and *in vivo*.

RESULTS: Although dysplastic cell identity remained unchanged, the cortactin KO organoids exhibited a decrease in cellular organization and multicellular protrusions, which are considered aggressive features when observed *in vitro*. When injected into the flank of nude mice, cortactin KO cells failed malignant transformation into adenocarcinoma and solid tumor formation with reduced recruitment of fibroblasts and macrophages. In addition, cortactin KO cells showed diminished exosome secretion levels, and adenocarcinoma development was impaired when exosome secretion was inhibited in cortactin wild-type dysplastic cells.

CONCLUSIONS: These data suggest that cortactin is a functional element of membrane dynamics, malignant changes, and exosome secretion in dysplastic cells, and solid gastric tumor formation associated with alteration of the tumor microenvironment. *(Cell Mol Gastroenterol Hepatol 2025;19:101490; https://doi.org/10.1016/j.jcmgh.2025.101490)*

Keywords: Cortactin; Dysplasia; Extracellular Vesicles; Gastric Cancer; Metaplasia; Organoid; Tumor Formation.

Understanding the biology of pre-cancer has been identified as one of the top challenges in early cancer detection research. Gastric cancer is the fifth leading cause of cancer-related deaths worldwide[1] and arises through a series of carcinogenic stages including metaplasia and dysplasia.[2] Dysplasia has been described as the last stage in epithelial gastric carcinogenesis, which occurs before invasive carcinomas develop and is often observed in metachronous cancers in patients.[3,4] Recent investigations by our group suggest that a stem cell population, first present in dysplasia, can drive malignant changes in precancerous lesions and the development of adenocarcinoma.[5,6] Although understanding the mechanism of malignancy can provide opportunities for early detection of precancerous lesions and identification of possible pathways for

*Authors share co-first authorship.

Abbreviations used in this paper: **ALI, air-liquid interface; BSA, bovine serum albumin; CISR, Vanderbilt Cell Imaging Shared Resource; Cttn, cortactin; DMEM, Dulbecco's Modified Eagle Medium; DMSO, dimethyl sulfoxide; DPBS, Dulbecco's phosphate-buffered saline; EVs, extracellular vesicles; F-actin, filamentous actin; FBS, fetal bovine serum; GM130, golgi matrix protein 130; H&E, hematoxylin and eosin; IF, immunofluorescence; ILVs, intraluminal vesicles; KO, knock-out; LAMP1, lysosomal associated membrane protein 1; MVBs, multivesicular bodies; NTA, nanoparticle tracking analysis; PBS, phosphate buffered saline; PDGFRα, platelet-derived growth factor receptor α; pERM, phosphorylated ezrin/radixin/moesin; PFA, paraformaldehyde; PO, propylene oxide; qPCR, quantitative polymerase chain reaction; RAB7, Ras-associated binding protein 7; RT, room temperature; SD, standard deviation; sgRNA, single guide RNA; TBST, Tris-buffered saline with Tween-20; TEM, transmission electron microscope; TPSR, Translational Pathology Shared Resource; WT, wild-type; ZO-1, zonula occludens-1.**

Most current article

2352-345X
https://doi.org/10.1016/j.jcmgh.2025.101490

intervention, the precise molecular mechanism for the evolution of precancerous dysplastic cells into cancer in the stomach is largely unknown.

In our previous work, we generated dysplastic organoid lines, termed as Meta4, derived from dysplastic glands in the stomach of mice with an activated *Kras* gene capable of driving gastric carcinogenesis.[6–9] These dysplastic organoid lines exhibit common cytological features seen in dysplastic tissues, including disorganized cellular patterning and complex budding structures, which are protrusions outward from the organoid composed of a single layer of cells forming a "bud" in 3-dimensional (3D) culture.[6] Moreover, a stem cell population in Meta4 organoids can evolve to adenocarcinoma *in vivo* when injected subcutaneously, accompanied by the recruitment of surrounding tumor microenvironment.[6] Additionally, we found high expression of the actin-binding protein, cortactin, localized to the apical membrane of the dysplastic organoids.[6,10]

Cortactin is a prominent regulator of the branched actin network,[11] and its overexpression is closely associated with poor prognosis in many epithelial cancers.[12–15] Cortactin binds to filamentous actin (F-actin) and the actin-nucleating Arp2/3 complex to stabilize branched actin networks, allowing the formation of actin-rich cellular protrusions such as lamellipodia and invadopodia, which are crucial to the aggressive behavior of cancer cells.[10,16–19] At actin-rich membrane sites, cortactin promotes docking of multivesicular bodies (MVBs), leading to enhanced release of small extracellular vesicles (EVs) known as exosomes.[18] This release of exosomes transfers biomolecules to the surrounding microenvironment[20] and enhances lamellipodia and invadopodia stability and function, cell migration and invasion, and tumor metastasis.[21–24] We have previously shown the accumulation of cortactin in the apical membrane of 3D-cultured dysplastic organoids and in the cell membrane protrusion at the leading edge of 2-dimensional (2D)-cultured dysplastic cells.[6] However, the function of cortactin in malignant transformation of dysplastic cells has not yet been investigated.

In this study, we investigated the role of cortactin in malignant transformation of dysplastic cells using dysplastic organoids. We found that cortactin knock-out (KO) dysplastic cells in 3D organoid cultures show a reduction in aggressive budding formation, multilayer growth and exosome secretion. *In vivo*, cortactin KO dysplastic cells failed to evolve into adenocarcinoma concomitant with a failure to recruit macrophages and fibroblasts to the microenvironment. These results collectively suggest a significant role for cortactin in modulating tumorigenicity of dysplastic cells during adenocarcinoma development.

Results

Cortactin is Differentially Expressed in Gastric Precancer and Cancer

To examine cortactin expression levels in each stage of gastric carcinogenesis, we immunostained for cortactin in a series of gastric tissues including normal, precancerous with metaplastic and dysplastic lesions, and cancerous. Cortactin protein was found diffusely in the cytoplasm and lowly expressed in the membrane of many normal gastric cells, while completely absent in metaplastic lesions (Figure 1*A*). In contrast, cortactin was highly expressed in the apical and basal membranes of glandular cells in dysplastic and cancerous tissues. Because cortactin in the cell periphery is known to promote lamellipodial dynamics and invadopodium formation,[18,25,26] high levels of cortactin expression in the cell membranes of dysplastic glands may suggest the potential contribution of cortactin to membrane dynamics and functional changes in gastric dysplastic and cancer cells.

Inhibition of Cortactin Activation Alters the Aggressive Morphology of Dysplastic Organoids

To assess the significance of cortactin in dysplastic organoid behavior, we conducted a long-term treatment of Meta4 organoids with curcumin, a naturally occurring compound known to have a cortactin deactivation effect.[27] It is known that cortactin is functionally active when a tyrosine residue (Tyr421) is phosphorylated and inactivated by direct interaction with PTPN1, a tyrosine phosphatase that dephosphorylates Tyr421.[27,28] Although Meta4 organoids treated with DMSO develop into complex, densely packed structures with outward buds at 3 weeks, which are common behavioral features of dysplastic organoids,[5,6] Meta4 organoids treated with curcumin for 2 weeks remained as cyst-like spheroids (Figure 1*B*). Seventy-four percent of dimethyl sulfoxide (DMSO)-treated Meta4 organoids developed outward budding structures, whereas only 13.3% of organoids exhibited cyst-like structures with inward budding (Figure 1*C and D*). In contrast, Meta4 organoids treated with curcumin resulted in a significant increase in inward budding formation, with more than 40% of the organoids having inward budding at a 50-μM dose of curcumin (Figure 1*D*). Hematoxylin and eosin (H&E) staining confirmed that bud tips mostly protruded outward from the organoids treated with DMSO, whereas curcumin-treated organoids were primarily found protruding into the hollow lumen (Figure 1*E*). Both DMSO- and curcumin-treated organoids displayed enlarged and disorganized nuclei, indicating that curcumin treatment only changed the behavior of dysplastic organoids and not the cytological characteristics of dysplasia (Figure 1*E*). Immunostaining for cortactin in paraffin-embedded organoid sections confirmed that peripheral enrichment of cortactin was decreased at the apical and lateral membranes and bud tips of organoids treated with curcumin (Figure 1*F and G*). In addition, the outward budding was significantly reduced (Figure 1*H*). These findings suggest that cortactin activity may be associated with the complex budding process of dysplastic organoids, which is considered an aggressive phenotype in 3D dysplastic organoid culture.[5,6]

Cortactin Determines the Aggressive Morphology of Dysplastic Organoids Without Disrupting Dysplastic Cell Identity

To directly investigate the role of cortactin (Cttn) in the dynamic behaviors of dysplastic cells, we utilized a CRISPR-Cas9 method in Meta4 organoids and generated an isogenic

organoid line. All surviving spheres after the CRISPR-Cas9 transfection were clonally expanded. A total of 49 clonal lines were expanded and screened, and one Cttn KO clone was successfully established with a 19-nucleotide deletion in exon 4 of the *Cttn* gene (Figure 2*A*). Loss of both Cttn mRNA expression and protein were confirmed by

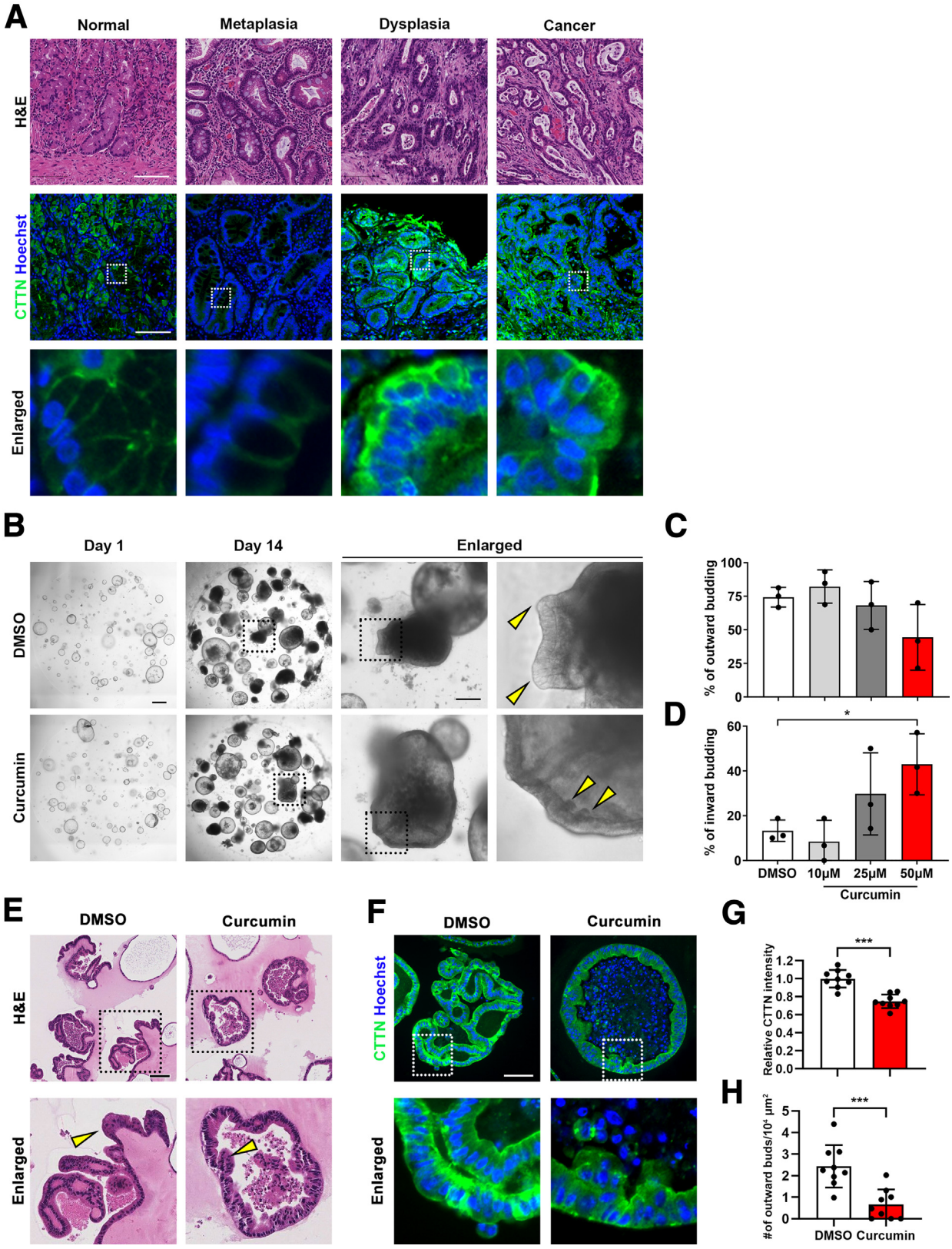

quantitative polymerase chain reaction (qPCR) and Western blot, respectively, confirming the loss of the *Cttn* gene and protein expression in the isogenic organoid line (Meta4-Cttn KO) compared with control Meta4 line (Meta4-Cttn wild-type [WT]) (Figure 2*B and C*). Both Meta4-Cttn WT and KO organoids grew into cyst-like structures within a week in 3D culture and formed advanced structures by 2 weeks (Figure 3*A*). The Meta4-Cttn KO organoids did not show any significant difference in growth rate and maintained dysplastic cell characteristics by sustained expression of a proliferation marker Ki-67 and dysplastic cell marker TROP2 (Figure 3*B*). Changes in mRNA expression for proliferation and genes associated with other gastric cell types were mostly unchanged (Figure 3*C and D*). At 2 weeks, more than 50% of Meta4-Cttn WT organoids formed outward budding structures, whereas fewer than 20% of Meta4-Cttn KO organoids formed such structures (Figure 3*E and F, left*). Additionally, Meta4-Cttn KO organoids exhibited a significant 2-fold increase in the number of organoids with inward buds compared with Meta4-Cttn WT organoids (Figure 3*F, right*), which is similar to the observed changes in curcumin treatment of Meta4 organoids. Therefore, these results suggest that cortactin is not involved in dysplastic cell growth or cellular identity but plays a critical role in the budding formation and cellular organization of dysplastic organoids.

Cortactin Controls Multicellular Protrusion and Apical Membrane Composition

Given that cortactin is a key molecule governing cell membrane dynamics by controlling actin branching in many types of cells including cancer cells,[19] we aimed to further understand the effect of cortactin on actin-dependent processes in precancerous cells. Transmission electron microscope (TEM) imaging of the organoids revealed a notable difference in microvilli formation after cortactin KO (Figure 4*A and C*). In addition, both γ-actin and phosphorylated ezrin/radixin/moesin (pERM), which are markers for actin-based microvilli stabilization and protrusion, are strongly upregulated at the plasma membrane of Meta4-Cttn WT cells and dramatically decreased in Meta4-Cttn KO cells (Figure 4*B*). However, mRNA levels of genes associated with actin and membrane formation, such as *Coro1b, Actg2, Myo5a, Myo5b, Ezrn, Stx3, Epcam, Cdh1, Espn,* and *Itga2* were unchanged (Figure 4*D*). These data confirm that cortactin primarily functions for membrane composition and protrusion formation in dysplastic cells.

To further assess alterations in epithelial growth behavior, we introduced an air-liquid interface (ALI) culture method, which allowed us to mimic the gastric epithelial environment *in vitro*, using Meta4-Cttn WT and KO organoids (Figure 5*A*). Dysplastic cells dissociated from Meta4-Cttn WT organoids formed a complicated multilayer structure with polypoid protrusions 4 weeks after initiation of the ALI culture (Figure 5*B and C, yellow arrowheads*), resembling the histologic phenotype of dysplasia observed in human patients.[29] In contrast, the loss of cortactin in Meta4 cells resulted in the formation of monolayer columnar cells without polypoid protrusions (Figure 5*B and C*). The top-down (or apical-basal) view of whole mount staining in ALI-cultures showed robust apical and intercellular F-actin staining in the Meta4-Cttn WT culture; however, this tumorigenic phenotype was diminished in the monolayered Meta4-Cttn KO cells (Figure 5*D*). Moreover, tight junctions labeled with zonula occludens-1 (ZO-1) and β-catenin were assembled in 4 weeks of ALI cultures of Meta4-Cttn KO cells (Figure 5*D*). These results suggest that multilayers and polypoid protrusions observed in long-term culture of dysplastic cells may be formed through cortactin-induced defects in apical-basal polarity, collectively considered an outcome of malignant transformation, and that cortactin is a regulator of the actin-mediated stabilization of multilayered structures.

We additionally examined the cellular dynamics of Meta4-Cttn WT and KO cells in 2D culture and found that cortactin expression was highly concentrated at the leading edge of WT cells where the cell membrane protruded (Figure 5*E*). However, the lamellipodia was not fully projected in dysplastic cortactin KO cells. Therefore, these data indicate that cortactin is a regulator in construction of both multilayered structures and polypoid protrusions, which may influence the histological structures of dysplasia observed in human stomach tissues.

Cortactin Facilitates Adenocarcinoma Development, Concomitant With Microenvironmental Cell Recruitment

In our previous studies, we demonstrated that *ex vivo* Meta4 organoids maintain the cellular characteristics of precancer when implanted back into the stomach wall of C57BL/6 mice. Furthermore, these organoids can progress

Figure 1. (***See previous page***). **Expression pattern and effect of cortactin inhibition in gastric dysplasia.** (*A*) H&E or IF stained images of human gastric tissues with multiple carcinogenic stages; normal, metaplasia, dysplasia, and cancer. *Dotted boxes* denote enlarged areas. (*B*) Phase contrast images of Meta4 organoids treated with or without 50 μM of curcumin for 2 weeks. *Yellow arrows* indicate the bud tips, and *dotted box* indicates the enlarged area shown next to it. (*C and D*) Quantification of the outward (*C*) or inward (*D*) budding ratio of Meta4 organoids after treatment with 10, 25, and 50 μM curcumin for 3 weeks. (*E*) H&E-stained images of Meta4 organoids treated with DMSO (vehicle) or 50 μM curcumin for 3 weeks. *Yellow arrows* indicate the bud tips, and *dotted boxes* indicate enlarged areas. (*F*) IF staining for cortactin in 50-μM curcumin treated Meta4 organoids. The nuclei were counterstained with Hoechst. *White dotted boxes* denote the enlarged areas. (*G and H*) Quantification of relative intensity of cortactin (*G*) or the number of outward buds per 10^4 μm^2 area (*H*) in Meta4 organoids treated with or without curcumin. Nine randomly selected images were used for analysis. All data are presented as mean $\pm$ SD (N = 3 if not stated). An unpaired 2-tailed *t*-test was used to assess *P*-value (*$P < .05$ and ***$P < .001$). Scale bars: 100 μm (*A and E*), 500 μm (*B, total views*), 200 μm (*B, enlarged images*) and 50 μm (*F*).

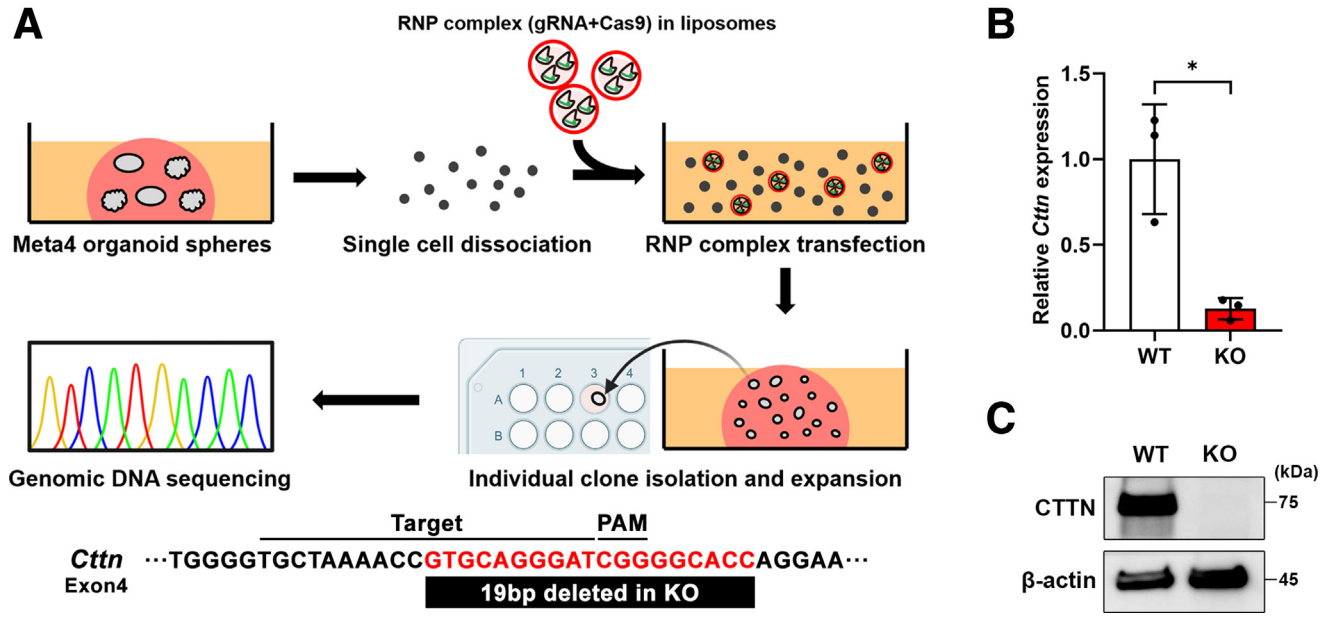

Figure 2. Establishment of cortactin KO Meta4 organoids. (*A*) Strategies of generation of an isogenic Meta4-Cttn KO line based on the CRISPR-Cas9 method. 19 nucleotides (red sequence) were deleted in the KO line; therefore, frameshift and early termination near the transcription start site occurred. (*B*) Relative cortactin mRNA expression in Meta4-Cttn KO Meta4 organoids to WT normalized to the expression of *Tbp*. (*C*) Western blot analysis for cortactin in Meta4-Cttn WT or KO organoids. All data are presented as mean ± SD (N = 3). Paired two-tailed *t*-test was used to assess *P*-value (*$P < .05$).

toward gastric adenocarcinoma when subcutaneously injected in immunodeficient nude mice.[5] Notably, we observed consistent expression of cortactin in the apical membranes of nearly all cells in Meta4 organoids.[6] To investigate the direct impact of cortactin on tumor formation ability, we conducted subcutaneous implantation using the Meta4-Cttn WT and KO organoids under the flanks of immunodeficient nude mice and examined their efficiency in initial engraftment formation. Six weeks after implantation, all implantation sites with Meta4-Cttn WT organoids had formed engraftments, whereas only 25% of Meta4-Cttn KO sites developed a small, engrafted lesion (Figure 6*A*). The engraftments derived from Meta4-Cttn WT organoids grew significantly in size over the 6 weeks, displaying fibrosis and cyst-like histology (Figure 6*B and C*).

However, the engraftment derived from Meta4-Cttn KO organoids remained very small and maintained dysplastic histology with no further growth or progression (Figure 6*B and C*). Furthermore, immunofluorescence staining of platelet-derived growth factor receptor α (PDGFRα), a fibroblast marker, showed that fibroblast cells were in close proximity to the epithelial-cell cysts in the Meta4-Cttn WT engraftments, but not around the Meta4-Cttn KO engraftment (Figure 6*D*). Additionally, the F4/80$^+$ macrophages were found close to the epithelial cells in engraftment of Meta4-Cttn WT and KO organoids (Figure 6*D*).

We further evaluated whether Meta4-Cttn KO organoids delay tumor development by monitoring the engraftment for a longer period of 13 weeks. Although Meta4-Cttn WT organoids progressed into bigger solid tumors, which reached humane endpoint in all mice, only 40% of Meta4-Cttn KO organoids developed small engraftments with the size of less than 5 mm^3, and none formed gross tumors (Figure 7*A and B*). The engraftments from Meta4-Cttn KO organoids did not continuously grow, and gross solid tumor formation was abrogated. Although many PDGRFα^+ fibroblasts and F4/80$^+$ macrophages were located adjacent to epithelial cells derived from Meta4-Cttn WT organoids, both fibroblasts and macrophages were highly reduced in Meta4-Cttn KO-derived engraftment and were not closely infiltrated to the epithelial cell area (Figure 7*C–F*). Furthermore, 20% of Meta4-Cttn WT tumors developed high-grade tubular adenocarcinoma with prominent stromal cells, but no adenocarcinoma was observed in Meta4-Cttn KO engraftments (Figure 7*G*). Additionally, the number of Ki-67$^+$/PDGRFα^+ cells, which were characterized as proliferative fibroblasts, decreased in the Meta4-Cttn KO engraftments (Figure 7*H and I*). To further confirm the effect of cortactin KO in dysplastic cells on fibroblast proliferation, we performed an indirect co-culture of fibroblasts isolated from dysplastic mucosa in Mist1-Kras mouse stomachs[7] with cells dissociated from Meta4-Cttn WT or KO organoids. The fibroblasts were immunostained for Ki-67 48 hours after the co-culture, and they were less proliferative in co-culture conditions with Meta4-Cttn KO cells. Consequently, the total number of fibroblasts was lower (Figure 7*J and K*). These results therefore support that cortactin promotes fibroblast proliferation, likely via cortactin-mediated secreted factors.

Collectively, these data reveal that cortactin is associated with solid tumor formation and adenocarcinoma development. The reduction in fibroblast and macrophage proximity to epithelial cells and the reduction in fibroblast proliferation following cortactin KO additionally suggests a role for cortactin in tumor microenvironment alterations.

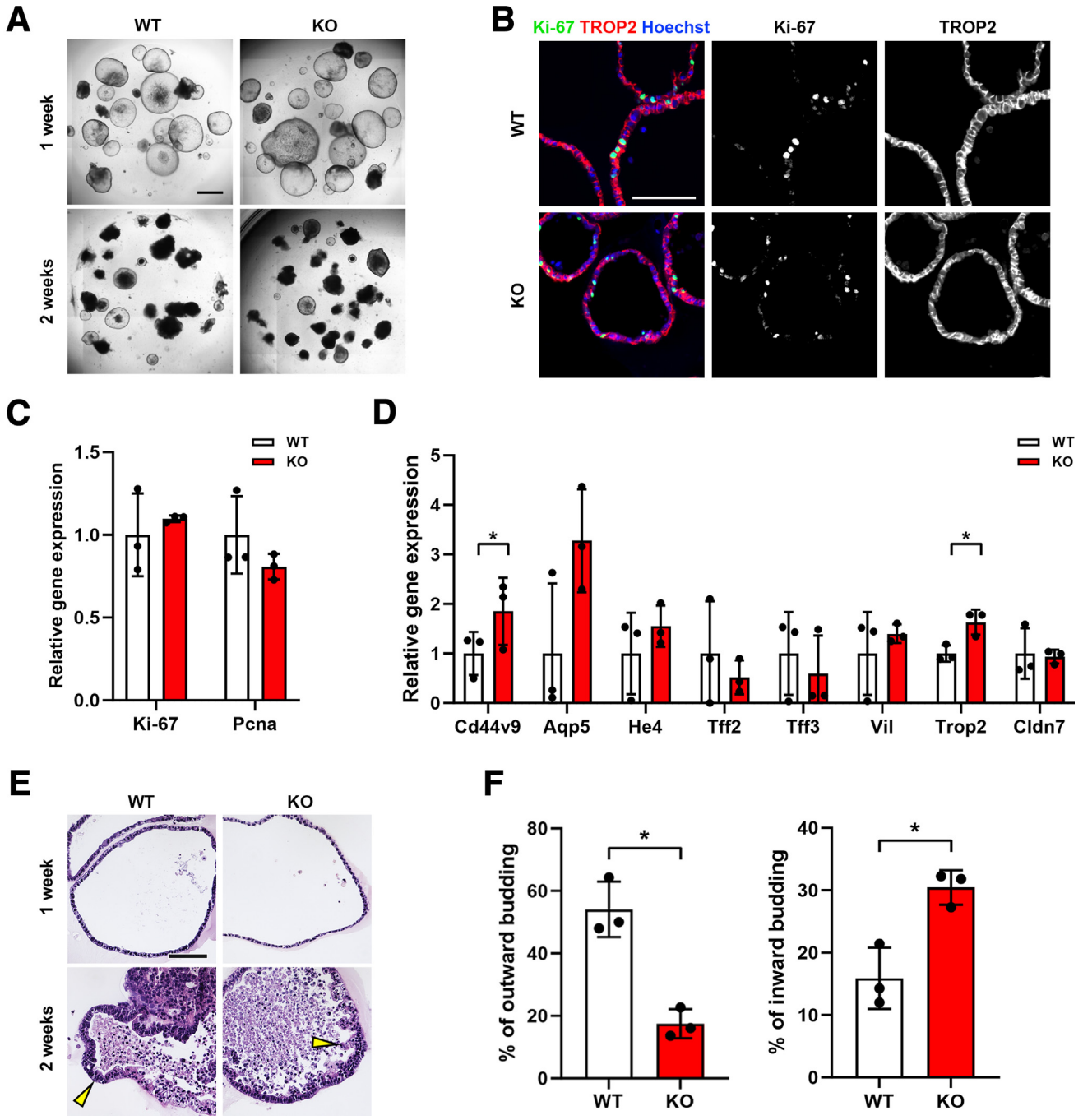

Figure 3. Changes in budding structure of Meta4 organoids after cortactin depletion. (*A*) Phase contrast images of Meta4-Cttn WT or KO organoids captured at 1 and 2 weeks after plating in ECM gel. (*B*) IF staining for Ki-67 and TROP2 in Meta4-Cttn WT or KO organoids. The nuclei were counterstained with Hoechst. (*C*) qPCR analysis of *Ki-67* and *Pcna* expression assessed in Meta4-Cttn WT or KO organoids. (*D*) Representative well-differentiated absorptive cell (*Vil*), metaplastic (*Cd44v9*, *Aqp5*, *He4,* and *Tff2*) and dysplastic (*Trop2* and *Cldn7*) lineage markers were quantified by qPCR assay in Meta4-Cttn WT or KO organoids. (*E*) H&E-stained images from Meta4-Cttn WT or KO organoids fixed at 1 or 2 weeks. *Yellow arrows* indicate the budded structures. (*F*) Quantification of outward (*left*) or inward (*right*) budding rate of Meta4-Cttn WT or KO organoids at 2 weeks. All data are presented as mean ± SD (N = 3). Paired two-tailed *t*-test was used to assess *P*-value (*$P < .05$). Scale bars: 1 mm (*A*), 50 μm (*B*), and 100 μm (*E*).

Cortactin Mediates Precancer Exosome Secretion

We previously showed that cortactin promotes docking of MVBs and release of exosomes from cancer cells.[21] This activity might account for the reduced recruitment of stromal cells in the *in vivo* microenvironment of Meta4-Cttn KO organoids.[30] To test whether there is a difference in exosome secretion in Meta4-Cttn WT and KO

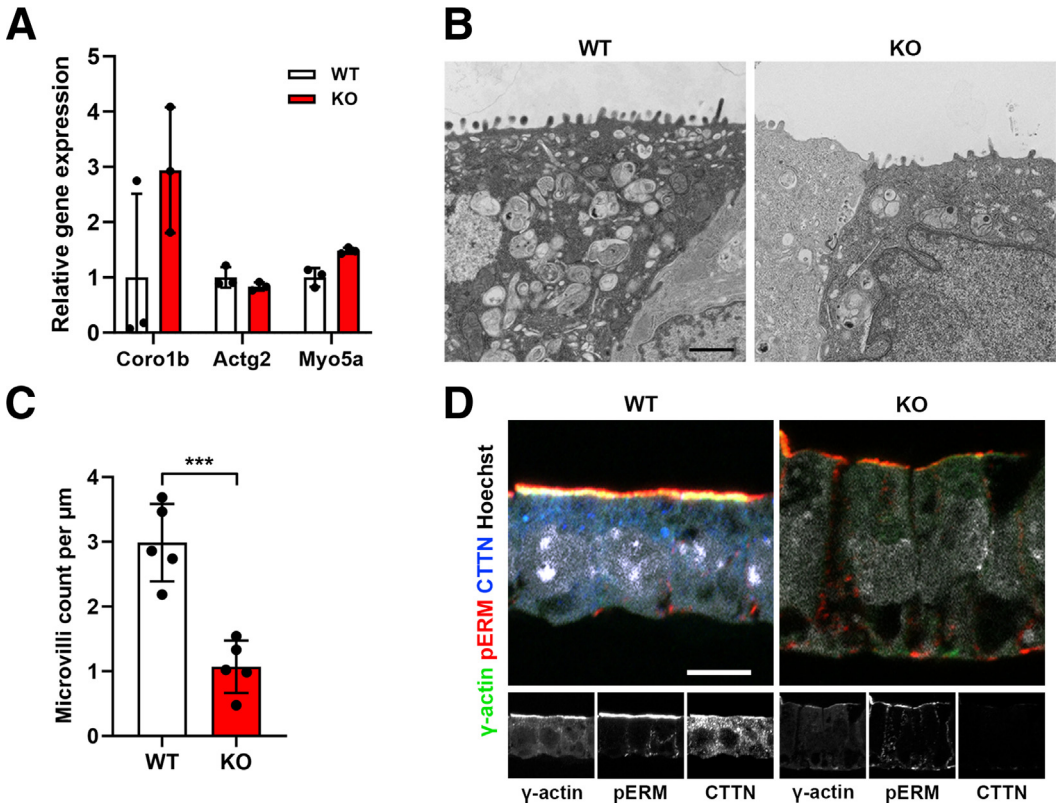

Figure 4. Cortactin-mediated regulation of microvilli protrusions and membrane composition in dysplastic organoids. (*A*) TEM images obtained from Meta4-Cttn WT or KO organoids. (*B*) IF staining for phosphorylated ERM, γ-actin, and cortactin of 3D-cultured Meta4-Cttn WT or KO organoids. The apical surface of the cells is oriented upwards in the images. All data are presented as mean ± SD. Paired (*A*) or unpaired (*C*) 2-tailed *t*-test was used to assess *P*-value (***$P < .001$). (*C*) The bar graph indicates the quantification of microvilli- like protrusions in Meta4-Cttn WT or KO organoids (N = 5). (*D*) Relative expression of representative actin and membrane dynamics-related genes analyzed by qPCR in Meta4-Cttn WT or KO organoids (N = 3). Scale bars: 1 µm (*A*) and 20 µm (*B*).

organoids, we carried out several experiments focused on exosome levels. By qPCR, we did not observe any significant differences in gene expression levels of exosome membrane markers *Cd9, Cd63,* and *Cd81* (Figure 8*A–C*). In addition, both CD9 and CD63 were localized in intracellular punctate compartments (Figure 8*B*), consistent with our previous finding that cortactin does not affect exosome biogenesis.[31] We also observed no changes in both *Alix* and *Tsg101* gene and protein levels (Figure 8*D and E*), which are components of the endosomal complexes known to be involved in exosome biogenesis and required for transport by (ESCRT)-I.[32] We next examined changes in markers associated with endosomal trafficking and exosome secretion in dysplastic organoids. A late endosomal compartment, the MVB containing intraluminal vesicles (ILVs) can either follow a lysosomal degradation pathway, or an exocytosis pathway leading to ILV release to extracellular area as exosomes.[33] Key factors of this process include Ras-associated binding protein 7 (RAB7), which directs late endosomes to merge with lysosomes,[34] lysosomal associated membrane protein 1 (LAMP1), which is a main component of lysosomal membrane,[35] and RAB27A, which is involved in the docking of MVBs to the plasma membrane.[31,36] The expression of *Lamp1* and *Rab7* genes was slightly increased in Meta4-Cttn KO organoids, and a prominent increase of LAMP1 and/or RAB7-positive puncta was also observed (Figure 8*F and G*). However, the *Rab27a* gene expression was decreased, and co-localization of RAB27A with cortactin at the apicolateral membrane was also abolished in Meta4-Cttn KO organoids, suggesting that cortactin stabilizes branched actin at the apicolateral membrane to enhance MVB docking by synchronizing with RAB27A (Figure 8*F and H*). Expression of other markers found in these secretion pathways were unaffected (Figure 8*I and J*). These data collectively suggest that the pathway related to exosome secretion may be altered in Meta4-Cttn KO organoids.

To determine whether exosome/small EV release is affected by cortactin KO, we performed TEM imaging using the organoids embedded in ECM gel, and the TEM images revealed that membranous vesicles were basolaterally secreted and trapped within ECM gel surrounding Meta4-Cttn WT organoids (Fig 9*A and B*). In contrast, we observed a reduction in secreted vesicles around the basolateral lumen in Meta4-Cttn KO organoids (Figure 9*A and B*). The secreted vesicles were lipid bilayered and cup-shaped, and the size distribution was between 80 and 120 nm, which are typical morphologic features of exosomes.[37]

We also directly quantified small EV secretion from the ALI culture of Meta4-Cttn WT and KO cells by collecting the conditioned media. To obtain enough material for analysis, the conditioned media was collected for 4 weeks, and large and small EVs containing exosomes were isolated through differential centrifugation. Western blots

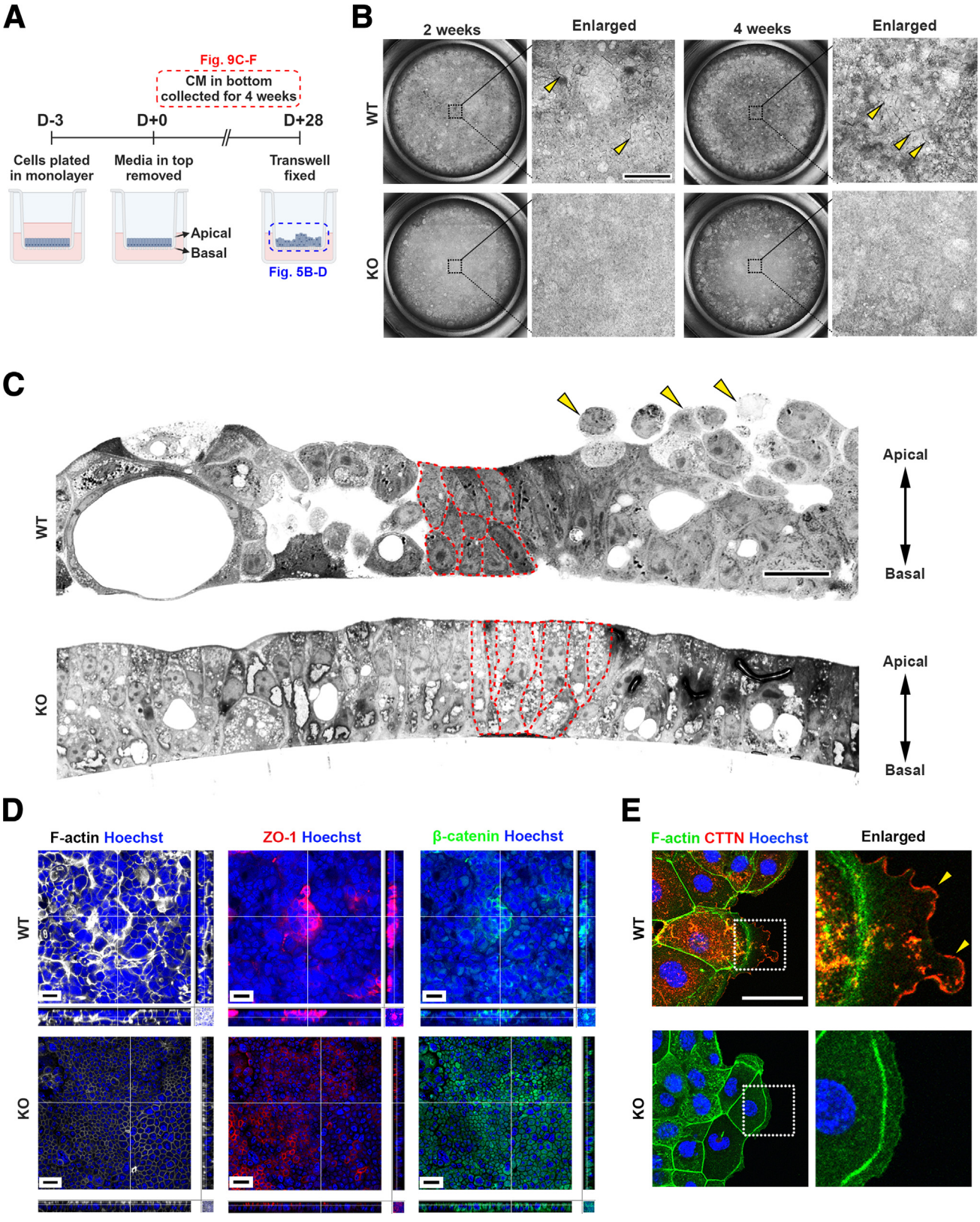

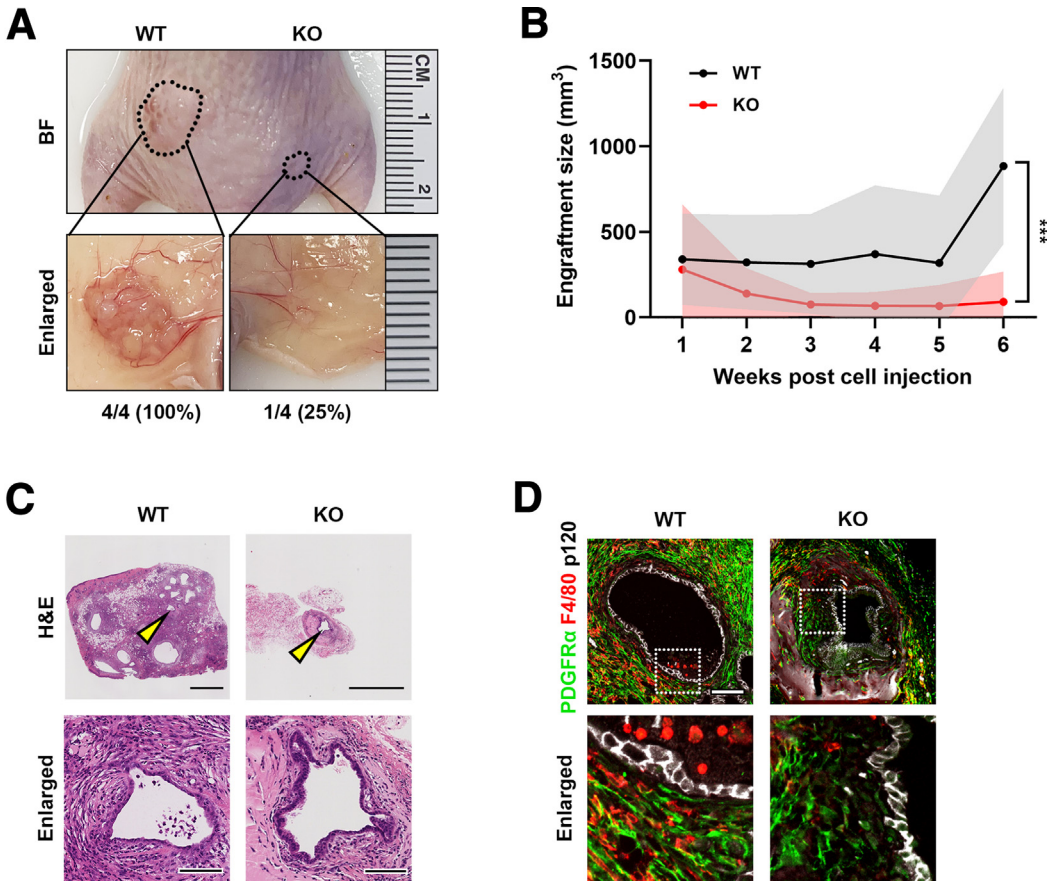

Figure 6. Characterization of dysplastic cell behavior *in vivo* according to cortactin expression at 6 weeks. (*A*) Gross images of tumor tissues 6 weeks after injection with Meta4-Cttn WT or KO organoids into nude mice. The dotted area represents the implant. (*B*) Growth over 6 weeks of engrafted tumors from injected Meta4-Cttn WT or KO organoids (N = 4). (*C*) H&E staining of tumor tissue from nude mice injected with Meta4-Cttn WT or KO organoids after 6 weeks. *Yellow arrows* indicate enlarged views. (*D*) IF staining for F4/80, PDGFRα, and p120 of tumor tissues excised at 6 weeks. All data are presented as mean ± SD. Unpaired 2-tailed *t*-test was used to assess *P*-value (***$P < .001$). Scale bars: 1 mm (*C, top*) and 100 μm (*C, bottom and D*).

with TSG101 and CD63, well-known small EV markers, or golgi matrix protein 130 (GM130), which is absent in exosomes,[38] validated the presence of small EVs in the conditioned media (Figure 9*C*). We found no difference in the quantity of large vesicles between the conditioned media from either Meta4-Cttn WT and KO cells, but the number of small EVs, indicating exosome-enriched fraction, from Meta4-Cttn KO cells was significantly decreased (Figure 9*D–F*). Therefore, these data collectively show that cortactin contributes to regulation of exosome release from dysplastic cells.

Exosome Secretion From Dysplastic Cells Mediates Fibroblast Recruitment and Adenocarcinoma Development

To further examine how cortactin-mediated exosome secretion influences the tumorigenicity of dysplastic cells and the recruitment of cells in the microenvironment, we inhibited exosome secretion during the dysplasia evolution *in vivo*. Because we already observed a significant decrease in RAB27 gene expression and a disruption in its specific localization at the apicolateral membrane in Meta4-Cttn KO organoids (Figure 8*F and H*), we utilized a small compound

Figure 5. (*See previous page*). Cortactin-mediated regulation of multicellular protrusions and membrane composition in ALI culture. (*A*) Schematic of ALI culture strategy and CM collection for secreted exosome study. (*B*) Phase contrast images in top-down (apical-basal) view captured at 2 or 4 weeks of Meta4-Cttn WT or KO organoids in ALI culture. *Dotted boxes* imply enlarged regions, and *yellow arrows* indicate protrusions. (*C*) Bright field images of thick sections from ALI cultured Meta4-Cttn WT or KO cells. *Yellow arrows* indicate protrusions, and *red dashed lines* indicate the cell plasma membrane. (*D*) Top-down (apical-basal) view of whole mount staining for F-actin, ZO-1, or β-catenin in ALI cultured Meta4-Cttn WT or KO cells with corresponding Z-axis images. (*E*) IF staining for cortactin and F-actin in monolayer-cultured Meta4-Cttn WT or KO cells. The *dotted box* indicates the enlarged area, and *yellow arrows* indicate protrusions of plasma membrane. The nuclei were counterstained with Hoechst. Scale bars: 300 μm (*B*), 20 μm (*C and D*), and 50 μm (*E*).

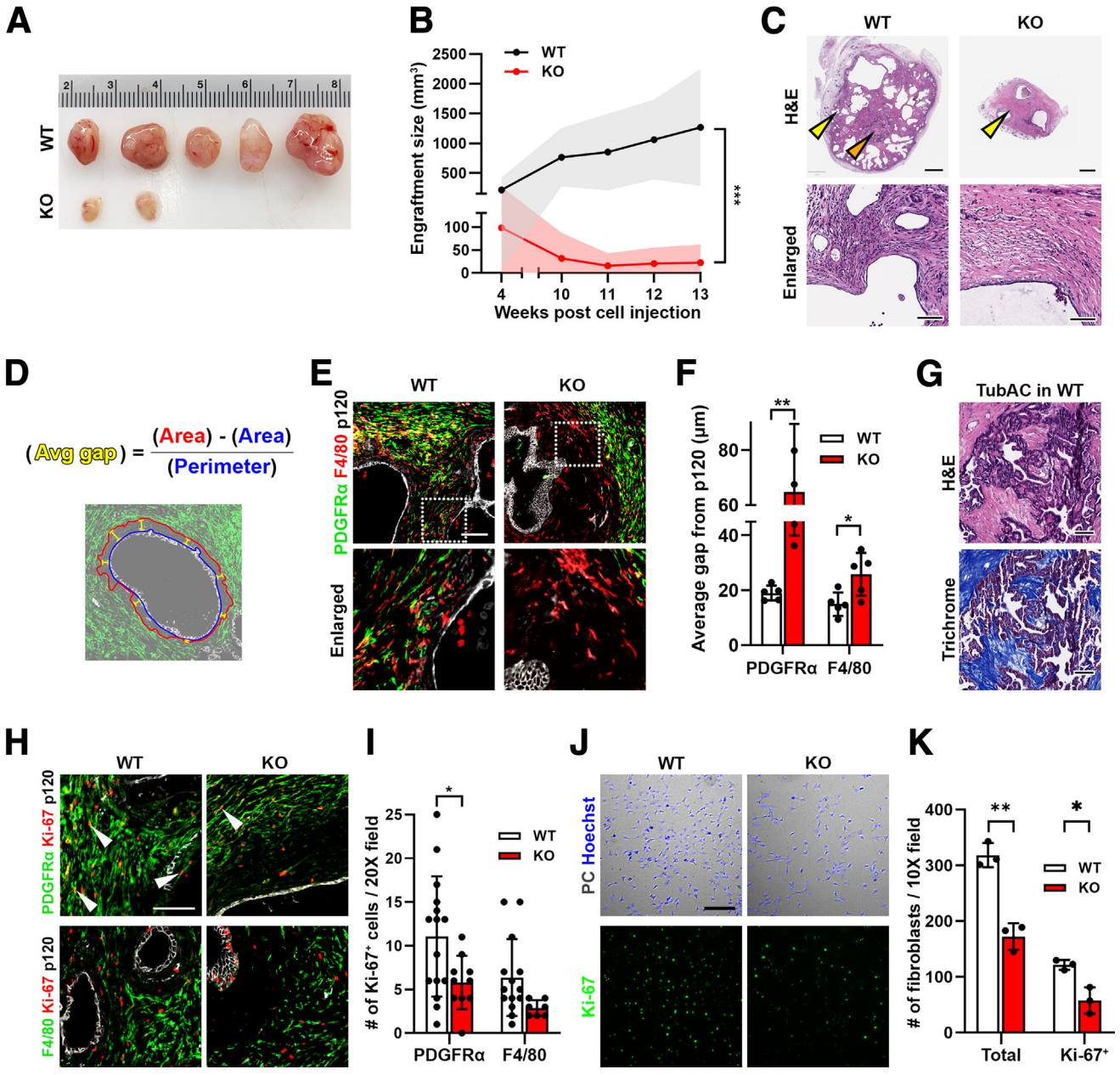

Figure 7. Characterization of dysplastic cell behavior *in vivo* according to cortactin expression at 13 weeks. (*A*) Bright field images of tumor tissues 13 weeks after injection (N = 5). (*B*) Tumor growth measured over 13 weeks in nude mice injected with Meta4-Cttn WT or KO organoids. (*C*) H&E-stained images of tumor at 13 weeks. *Yellow and orange arrows* denote enlarged views in *C* and *G*, respectively. (*D*) Quantitation strategies of average gap between p120 (epithelial cells) and PDGFRα (fibroblasts) or F4/80 (macrophages). (*E*) IF staining for PDGFRα, F4/80, and p120 of tumor tissues excised at 13 weeks. (*F*) Quantitation of average gap between p120 and each marker. Five epithelial cell areas were randomly selected from each of Meta4-Cttn WT or KO organoids injected groups to analyze average gaps. (*G*) Tubular adenocarcinoma area of the Meta4-Cttn WT organoid-injected group stained with H&E and Masson's trichrome. (*H*) IF staining of PDGFRα, F4/80, Ki-67, and p120 of 13 weeks tumor tissues from Meta4-Cttn WT or KO organoid injections. *White arrows* denoted cells co-positive with PDGFRα and Ki-67. (*I*) Quantification of number of PDGFRα^+ or F4/80$^+$ cells that are co-positive with Ki-67 per each 20$\times$ field. Fifteen images randomly selected IF images were analyzed. (*J*) Phase contrast (PC) image overlayed with IF staining of Hoechst and Ki-67 of fibroblasts after 2 days of indirect co-culture with Meta4-Cttn WT or KO cells on top of the Transwell. (*K*) Quantification of number of total fibroblasts or Ki-67 positive fibroblasts per 10$\times$ field. Three independent experiments conducted. All data are presented as mean $\pm$ SD. Unpaired 2-tailed *t*-test was used to assess *P*-value (*$P < .05$; **$P < .01$; and ***$P < .001$). Scale bars: 1 mm (*C, Top*), 100 μm (*E, G, H and bottom images of C*), and 200 μm (*J*).

inhibitor, Nexinhib20, that blocks the docking of RAB27A-containing endosomes to the plasma membrane.[39] We first treated Meta4 organoids with 5 μM Nexinhib20 and observed no significant changes in morphology and size of organoids after 3 days (Figure 10*A and B*). Conditioned media from ALI-cultured Meta4 cells, treated with or without Nexinhib20, were collected over 2 weeks and centrifuged at 100,000 $\times$ *g*. A nanoparticle tracking analysis

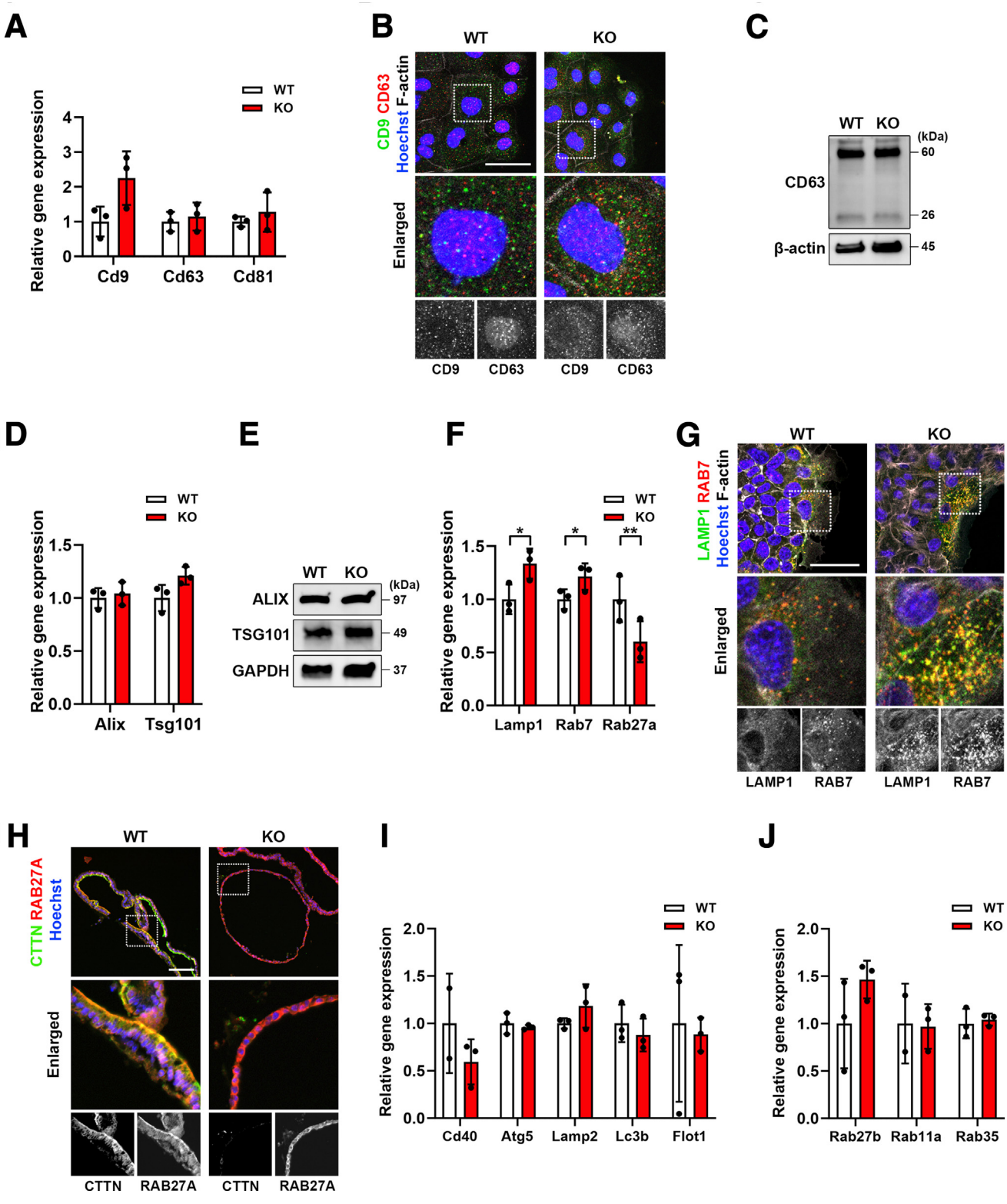

of Nexinhib20-treated media revealed a nearly 2-fold reduction in exosome numbers (Figure 10*C*), suggesting that Nexinhib20 inhibits exosome secretion from dysplastic cells without affecting organoid growth. To examine the effects of secreted exosomes *in vivo*, Meta4 dysplastic organoids were first subcutaneously injected into the flanks of nude mice. At 4 weeks after the injection, the nude mice were intraperitoneally administered with 2.5 mg/kg Nexinhib20 for 6 weeks. Solid tumor sizes were significantly smaller in the Nexinhib20-treated group (Figure 10*D and E*), and H&E staining confirmed reduced recruitment of stromal cells to cystic or adenocarcinoma lesions (Figure 10*F and I*). Although F4/80$^+$ macrophages did not show any significant changes, PDGFRα^+ fibroblasts were located significantly farther from p120$^+$ epithelial cysts in the Nexinhib20-treated group (Figure 10*G and H*). These results support the *in vivo* results from Meta4-Cttn KO (Figures 6 and 7) but suggest a different mechanism by which cortactin affects macrophage recruitment. Although all solid tumors displayed the histologic features of tubular adenocarcinoma, the area size of tubular adenocarcinoma lesions was significantly reduced in the solid tumors treated with Nexinhib20 with the reduction in fibrosis (Figure 10*I and J*). Taken together, these findings suggest that decreased exosome secretion after Nexinhib20 treatment impairs solid tumor growth and the ability of dysplastic cells to recruit PDGFRα^+ fibroblasts. Nevertheless, the persistent tumorigenicity and presence of tubular adenocarcinoma lesions in the Nexinhib20-treated group suggest a complex role of cortactin in dysplastic cell evolution and tumorigenesis beyond the regulation of exosome secretion.

Discussion

Cell behavioral changes through membrane dynamics and recruitment of stromal and immune cells in carcinogenesis have been recognized as pivotal factors in the progression to cancerous stages.[40] In this study, we identified cortactin as an important factor that regulates dysplastic cell function to acquire malignancy in the stomach, leading to the evolution of pre-cancerous dysplastic cells into adenocarcinoma. Although cortactin has been studied primarily in cancer for its role in promoting cancer cell migration and invasion,[10,41–44] here, we observed the increased expression and localization of cortactin to plasma membranes in dysplastic cells, compared with normal gastric and metaplastic cells (Figure 1*A*). We also found that cortactin promotes aberrant architecture (Figure 3*E*, 4*A*, and 5*C*) and exosome secretion (Figure 9) of dysplastic cells. In addition, *in vivo* cortactin KO dysplastic cells recruited fewer macrophages and fibroblasts to their environment and failed to transform into adenocarcinoma and to develop solid tumors (Figures 6 and 7).

We leveraged an organoid model system to monitor alterations in cellular and multicellular phenotypes of dysplastic cells within a 3D-cultured environment. Both inhibition of cortactin activation and endogenous knock-out of cortactin in dysplastic organoids significantly reduced outward budding formation, which is achieved by protrusion into the ECM gel matrix, a common behavioral feature of dysplastic organoids (Figures 1*E* and 3*E*). These results align with a reduction in membrane protrusions (Figure 5*E*) that serves as an initiating stage for cell migration. The observed inward budding into the lumen was presumably due to the loss of protrusions into the ECM gel matrix by cortactin KO in dysplastic organoids. Although cortactin KO cells did not display changes in mRNA levels of actin and membrane-associated genes, the cells displayed significant loss of microvilli formation, and changes in the protein composition of the membrane as expected because cortactin is not a transcriptional regulator (Figure 4*A–D*). Therefore, cortactin is likely a major contributor to dysplastic cell membrane function and behavior.

The dysplastic cells also exhibit polypoid projections with irregular multilayered cell structures in ALI cultures.[29] However, in cortactin KO dysplastic cells, these projections were absent, with cells forming monolayers with distinct apical and basolateral orientations (Figure 5*B–D*). Because aberrant control of membrane dynamics is highly associated with aggressive behaviors of cancer cells,[45,46] these findings indicate that many abnormal behavioral features that define the dysplastic stage[47] are governed, at least partially, by cortactin. It should be noted that only a single cortactin KO clone was used to examine multiple roles of cortactin during dysplasia evolution to adenocarcinoma, which is a potential limitation of this study as the possibility of clonal variation cannot be fully ruled out. Therefore, further studies using transgenic animal models are required to fully understand the roles of cortactin in dysplastic cells.

Figure 8. (***See previous page***). **Examination of exosome related markers in cortactin WT and KO dysplastic cells.** (*A*) Relative expression of exosome membrane markers (*Cd9*, *Cd63,* and *Cd81*) quantified by qPCR assay in Meta4-Cttn WT or KO organoids. (*B*) IF staining for CD63 and CD9 in Meta4-Cttn WT or KO monolayer cells. *Dotted boxes* indicate enlarged areas. (*C*) Western blots of CD63 in Meta4-Cttn WT or KO organoids. β-actin as a house-keeping gene control. (*D*) Relative expression of exosome formation markers (*Alix* and *Tsg101*) in Meta4-Cttn WT or KO organoids, as examined by qPCR and normalized to the expression of *Tbp*. (*E*) Western blots of ALIX and TSG101 in Meta4-Cttn WT or KO organoids. GAPDH as a house-keeping gene control. (*F*) Relative expression of lysosomal marker (*Lamp1*), vesicle trafficking markers (*Rab7* and *Rab27a*) quantified by qPCR assay in Meta4-Cttn WT or KO organoids. (*G*) IF staining for LAMP1 and RAB7 in Meta4-Cttn WT or KO monolayer cells. *Dotted boxes* indicate enlarged views. The nuclei were counterstained with Hoechst. (*H*) IF staining for cortactin and RAB27A in Meta4-Cttn WT or KO organoids. *Dotted boxes* indicate enlarged views. The nuclei were counterstained with Hoechst. (*I*) qPCR analysis of representative expression of vesicle trafficking-related genes in Meta4-Cttn WT or KO organoids. (*J*) qPCR analysis of *Rab27b*, *Rab11a,* and *Rab35* in Meta4-Cttn WT or KO organoids. All data are presented as mean $\pm$ SD (N = 3). Paired 2-tailed *t*-test was used to assess *P*-value (*$P < .05$ and **$P < .01$). Scale bars: 50 μm (*B and G*), 100 μm (*H*).

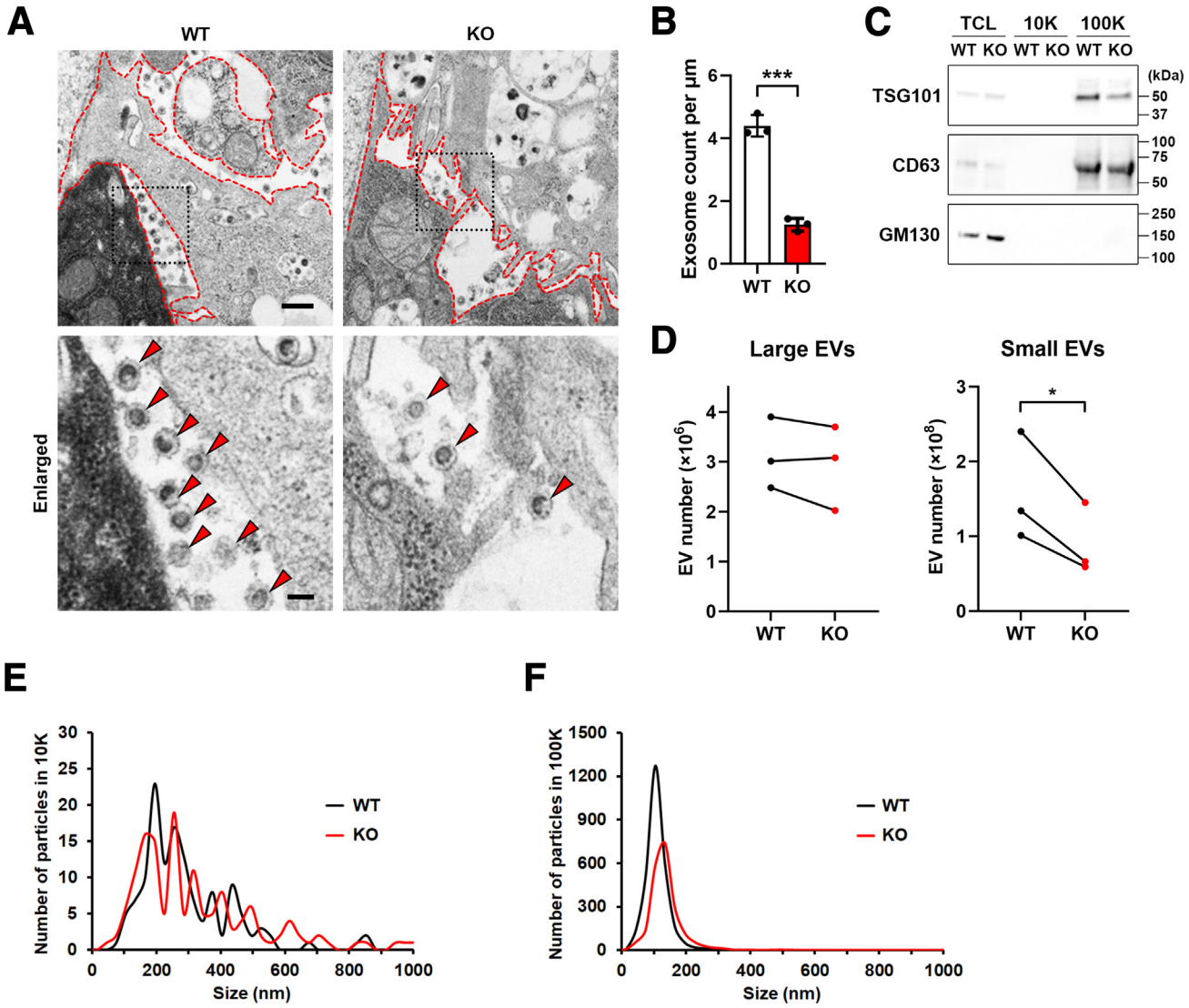

Figure 9. Quantification of exosome secretion from cortactin WT and KO dysplastic cells. (*A*) TEM images of exosomes secreted from Meta4-Cttn WT or KO organoids in 3D culture. *Red dashed lines* in top panels indicate the boundaries of cells, and *black dotted boxes* indicate enlarged areas. *Red arrows* in enlarged images indicate the secreted exosomes. (*B*) Quantification of exosomes trapped in ECM gel from TEM imaging. Exosomes were quantified by counting number per μm of cell membrane in areas containing exosomes. (*C*) Western blot performed for the expression of TSG101, CD63, and GM130 in secreted EVs from Meta4-Cttn WT or KO ALI cultures. TCL, total cell lysates; 10K, pellets from 10,000 $\times$ *g* centrifugation for 30 minutes; 100K, pellets from 100,000 $\times$ *g* centrifugation for overnight. (*D*) Quantification of number of secreted large EVs or small EVs from the CM of ALI-cultured Meta4-Cttn WT (*black dots*) or KO (*red dots*). (*E and F*) Nanoparticle tracking analysis of 10,000 $\times$ g (*E*) or 100,000 $\times$ g (*F*)-centrifuged CM collected from Meta4-Cttn WT or KO ALI cultures. All data are presented as mean $\pm$ SD (N = 3). An unpaired (*B*) or paired (*D*) 2-tailed *t*-test was used to assess *P*-value (*$P < .05$ and ***$P < .001$). Scale bars: 400 nm (*A, top*) and 100 nm (*A, bottom*).

We also found that cortactin KO in dysplastic cells significantly inhibited not only solid tumor formation but also adenocarcinoma development *in vivo* upon injection subcutaneously into mice (Figures 6*A and B*, 7*A and B*). As cortactin has no effects on the proliferative activity or identity of the dysplastic cells (Figure 3*B–D*), we suspected a cell-non-autonomous effect. Moreover, even when cystic engraftments developed after Meta4-Cttn KO cell injection, recruitment of fibroblasts and macrophages were notably reduced around the lesions (Figures 6*D*, 7*E and F*). Stromal cells facilitate tumor progression by providing an optimal niche, including structural support and an immune-suppressive environment.[48] One mechanism by which tumor cells communicate with cells in their microenvironment, including stromal cells and macrophages, is via EVs.[49–51] Consistent with our previous finding that cortactin affects MVB docking and exosome secretion,[31] here, we found that loss of cortactin results in a decrease in the number of small EVs released from dysplastic cells. We also found that cortactin KO led to

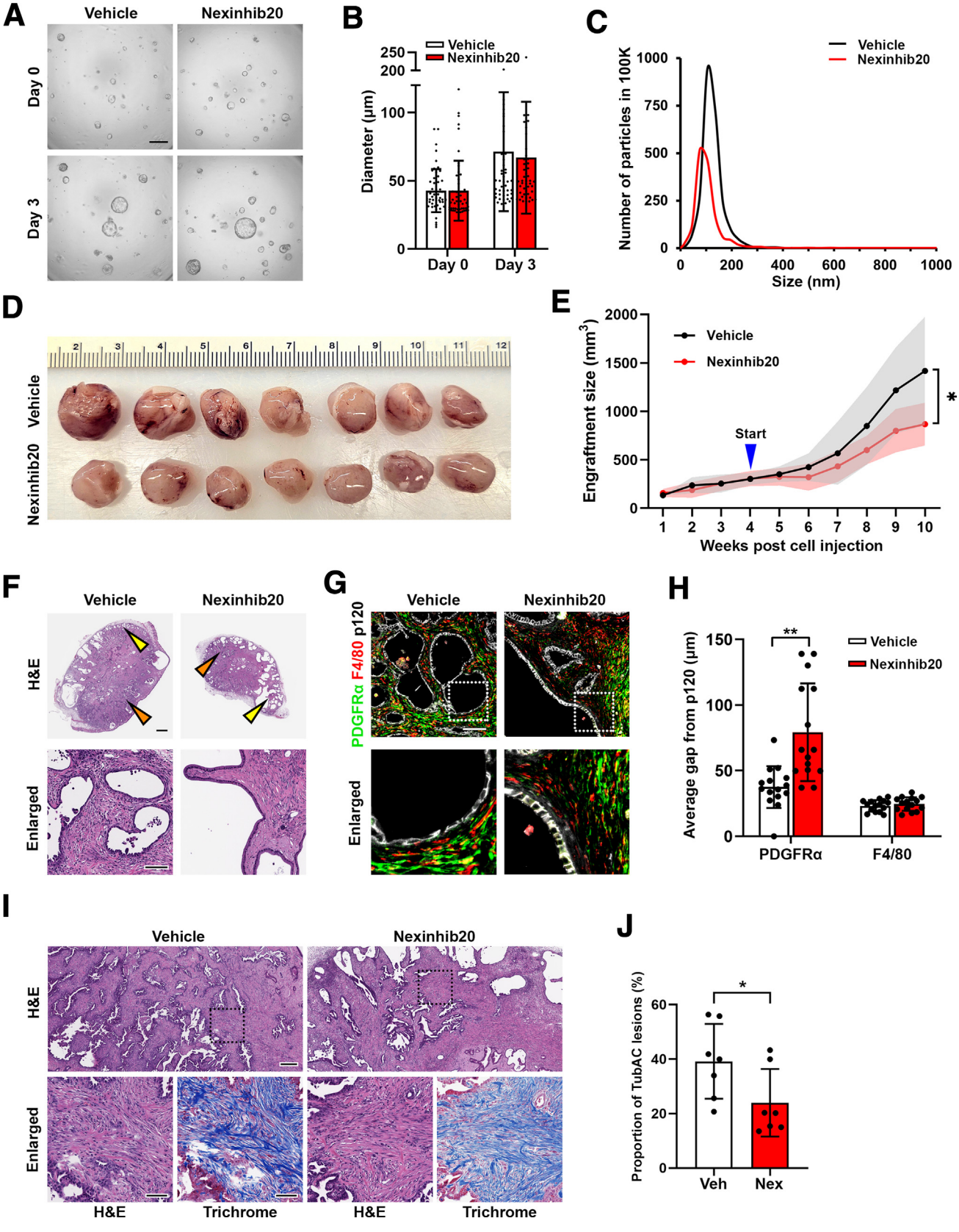
A
Vehicle
Nexinhib20
Day 0
Day 3
B
Vehicle
Nexinhib20
Diameter (µm)
250
200
100
50
0
Day 0
Day 3
C
Vehicle
Nexinhib20
Number of particles in 100K
1000
750
500
250
0
0
200
400
600
800
1000
Size (nm)
D
Vehicle
Nexinhib20
E
Engraftment size (mm3)
2000
1500
1000
500
0
Vehicle
Nexinhib20
Start
*
1
2
3
4
5
6
7
8
9
10
Weeks post cell injection
F
Vehicle
Nexinhib20
H&E
Enlarged
G
Vehicle
Nexinhib20
PDGFRα F4/80 p120
Enlarged
H
Average gap from p120 (µm)
150
100
50
0
**
Vehicle
Nexinhib20
PDGFRα
F4/80
I
Vehicle
Nexinhib20
H&E
Enlarged
H&E
Trichrome
H&E
Trichrome
J
Proportion of TubAC lesions (%)
60
40
20
0
*
Veh
Nex

alterations in the gene expression level and localization of the MVB docking factor RAB27A (Figure 8*F and H*), further suggesting perturbation of exosome secretion. Because exosomes facilitate tumor growth and recruitment of stromal cells,[52] cortactin-mediated exosome secretion may be a crucial factor in dysplastic cell evolution to adenocarcinoma *in vivo*. The *in vivo* inhibition of exosome secretion by Nexinhib20 also reduced fibroblast recruitment and decreased tubular adenocarcinoma development (Figure 10*D–J*). However, Nexinhib20 treatment did not fully replicate the effects seen in the cortactin KO experiments, which suggests that cortactin may have multiple roles contributing to the progression of dysplasia to adenocarcinoma. In addition, the Nexinhib20 treatment did not impact macrophage recruitment *in vivo* (Figure 10*G and H*). Although it is known that macrophages can be recruited to the tumor regions via exosomal cargos,[49] our data may suggest an additional function of cortactin in macrophage recruitment that is separate from exosome signaling. It needs to be noted that tumor size variability occurred between the cortactin KO injection (Figure 6) study and the Nexinhib20 injection study (Figure 10), due to the varying number of cells in individual organoids. Still, tumors between experiments were histologically identical, and statistically significant differences were found in both, validating our findings.

Conclusion

Our study suggests that cortactin is an essential protein in the evolution of dysplastic cells to adenocarcinoma in the stomach. Cortactin is critical for dysplastic cells to exhibit abnormal cellular organization and architecture, including multicellular protrusions, membrane composition, and complex outward budding structures. Notably, cortactin plays a pivotal role in establishing a pro-tumor microenvironment and promoting the progression of precancerous cells to malignancy, potentially through an exosome-mediated cell communication mechanism. Thus, our findings elucidate several of the biological mechanisms of cancerous cell lineage evolution from dysplastic cells and suggest that cortactin localization and/or expression may serve as a marker of dysplastic cells with high risk for conversion to malignancy.

Methods

Immunofluorescence staining

Stomach tissues were collected from patients with gastric cancer who underwent surgery at Seoul National University Hospital, Seoul, Korea (IRB No. H-1209-037-424). Tissues were fixed in 10% neutral buffered formalin for 5 to 7 days at room temperature (RT). Organoids grown in Matrigel were fixed in 4% paraformaldehyde (PFA) for 30 minutes at RT and embedded in HistoGel (Thermo Fisher Scientific). The fixed tissues and organoids were embedded in paraffin and sectioned at 5-μm thickness following a standard protocol at the Translational Pathology Shared Resource (TPSR) core facility at Vanderbilt University Medical Center. Tissue or organoid sections were deparaffinized in Histoclear and rehydrated in ethanol. Antigen retrieval was performed in a pressure cooker in Target Retrieval Solution (Dako) and sections were then blocked with Protein Block Serum-Free solution (Dako) for 1.5 hours at RT. Sections were applied with primary antibodies diluted in Antibody Diluent (Dako) at 4 °C overnight and washed in phosphate buffered saline (PBS). Alexa-conjugated secondary antibodies (Life Technologies, 1:500) diluted in Antibody Diluent (Dako) were then applied for 1 hour at RT, washed in PBS, and nuclear stained with Hoechst (Thermo Fisher Scientific, 1:10,000). The fluorescence images were acquired with a ZEISS Axio Imager M2 microscope. Antibodies used for immunostaining are listed in Table 1.

Organoid Culture and Treatment

All organoid-related experiments were performed using established dysplastic organoid lines, Meta4, isolated from Mist1-Kras mouse stomachs, cultured as previously described.[6] Briefly, Meta4 was passaged in ECM gel (Sigma-Aldrich) with IntestiCult Intestinal Organoid Growth Medium (Mouse, StemCell Technology) containing 1% penicillin/streptomycin (Gibco) and incubated in 37 °C humidified chamber. To culture Meta4 dysplastic cells into 2D monolayer, the organoids were dissociated with TrypLE Express Enzyme (Gibco) for 5 minutes at 37 °C and passed through a 100-μm cell strainer. Dissociated cells were plated on an 8-well tissue culture plate (Ibidi) treated with collagen I at 5000 cells per well and maintained with Mouse IntestiCult media.

Figure 10. (***See previous page***). **Examination of roles of exosomes in dysplastic cells tumorigenicity *in vivo* using exosome secretion inhibitor Nexinhib20.** (*A*) Phase contrast images of Meta4 organoids treated with or without 5 μM Nexinhib20 for 3 days. (*B*) Quantification of diameter of 50 organoid sphere after 3 days of vehicle or Nexinhib20 treatment. (*C*) Nanoparticle tracking analysis of 100,000 × *g*-centrifuged CM collected from the pooled 3 samples of Meta4 ALI cultures treated with vehicle or Nexinhib20 for 2 weeks. (*D*) Bright field images of tumor tissues after 4 weeks of Meta4 organoid injection followed by 6 weeks of vehicle or Nexinhib20 injection (N = 7). (*E*) Tumor growth measured over 10 weeks in nude mice (N = 7). (*F*) H&E-stained images of tumor at 10 weeks. *Yellow and orange arrows* denote enlarged views in *F* and *I*, respectively. (*G*) IF staining for PDGFRα, F4/80, and p120 of tumor tissues excised at 10 weeks. (*H*) Quantitation of average gap between p120 and each marker. Fifteen of epithelial cell areas were randomly selected from each of vehicle or Nexinhib20 injected groups to analyze average gaps. (*I*) Tubular adenocarcinoma area of the vehicle or Nexinhib20 injected group stained with H&E and Masson's trichrome. *Black dotted boxes* denote enlarged views. (*J*) Proportion of tubular adenocarcinoma developed regions per each tissue section area (N = 7). All data are presented as mean ± SD. An unpaired 2-tailed *t*-test was used to assess *P*-value (*$P < .05$ and **$P < .01$). Scale bars: 200 μm (*A*),1 mm (*F, top*), 100 μm (*G and enlarged images in F and I*), and 300 μm (*I, top*).

To evaluate the effect of cortactin deactivation in the organoids, curcumin, reconstituted in DMSO, was added at a final concentration of 50 μM to the Mouse IntestiCult media without Y-27632, 1 or 2 days after plating. Media containing either DMSO or 50 μM of curcumin was replaced every 3 days for 2 weeks. To examine the proliferative activity of fibroblasts co-cultured with cortactin WT or KO Meta4 cells, single-cell-dissociated Meta4 cells were plated on top of the collagen-coated Transwell until they became confluent. After 3 days, 10,000 fibroblasts established from the stomachs of Mist1-Kras mice (see detailed procedure below) were plated in a 24-well plate and indirectly co-cultured with Meta4-plated Transwell for 2 days. To test cytotoxicity of Nexinhib20 on Meta4 cells, DMSO or 5 μM Nexinhib20-containing Mouse IntestiCult media was treated to 3D-cultured Meta4 for 3 days (Figure 10*A and B*). To inhibit exosome secretion from Meta4 cells, air-liquid interface (ALI)-cultured Meta4 cells (see detailed method below) were treated with DMSO or for 5 μM Nexinhib20 for 2 weeks (Figure 10*C*). Phase-contrast images were captured using an EVOS M7000 (Invitrogen) inverted microscope.

Fibroblast Isolation

Fresh mouse stomach tissues were harvested from Mist1-Kras-mTmG mice,[7] and stomach mucosa was separated from the muscle layer using a cell scraper. A grid pattern was scored in wells in a 6-well plate using a sterile razor blade, and minced mucosa was moved to the wells. The plate containing minced mucosa was incubated at 37 °C for 30 minutes, then Dulbecco's Modified Eagle Medium (DMEM) F12 (Corning) with 10% fetal bovine serum (FBS) added to each well. After the fibroblasts crawled out from the anchored mucosa, the remaining mucosa was removed, and the fibroblasts were maintained in DMEM F12 supplemented with 10% FBS.

Generation of Cortactin KO Organoids

Meta4 organoids were plated and grown for 4 days in a 48-well plate. The organoids were first broken into small pieces, followed by a PBS wash, and the organoid chunks were centrifuged at 300 $\times g$ for 5 minutes. The pellets were resuspended in TrypLE (Gibco) supplemented with 0.1% Y-27632 and incubated for 5 minute at 37 °C for single-cell dissociation. The dissociated cells were centrifuged at 300 $\times$g for 5 minutes, followed by a PBS wash. Cell numbers were counted using a TC20 Automated Cell Counter (BioRad), and 10,000 viable cells were resuspended in Opti-MEM reduced serum-free media (Gibco). Transfection of TrueGuide Synthetic single guide RNA (sgRNA) for the mouse *Cttn* gene (Invitrogen) and TrueCut Cas9 Protein v2 (Invitrogen) was carried out using the Lipofectamine CRISPRMAX Reagent kit (Invitrogen). The mixture of sgRNA for *Cttn*, Cas9 protein, and the lipofectamine reagents was added to cells resuspended in the Mouse IntestiCult media supplemented with 1% of penicillin/streptomycin and 0.1% of Y-27632. As a control, the same number of cells were transfected with Cas9 protein and lipofectamine reagents without sgRNA. Each cell suspension was plated in 1 well of a 48-well plate. After 24 hours of incubation at 37 °C, the cells were centrifuged at 600 $\times g$ for 5 minutes and plated with ECM gel. Once the single cells grew into spheres, individual spheres were manually isolated using a pipette and plated in a 96-well plate. Spheres were split and transferred to a 48-well plate to expand the spheres from the same clone. Genomic DNA was extracted with lysis buffer containing proteinase K, precipitated and washed using isopropanol and 70% ethanol, respectively. gDNA PCR was performed using the Platinum II Hot-Start PCR Master Mix (Invitrogen). The deletion of the targeted sequences (5′-TGCTAAAACCGTGCAGGGATCGG) was confirmed by Sanger sequencing using the forward primer. A schematic diagram

Table 1. Antibody List

Antibody	Reference number	Source	Concentration	Assay
TSG101	ab30971	Abcam	1:1,000	WB
CD63	ab68416	Abcam	1:500	WB
GM130	610822	BD-Biosciences	1:250	WB
Cortactin	05-180-I	Millipore	1:1,000	IF
TROP2	AF650	R&D Systems	1:500	IF
Ki-67	652402	Biolegend	1:250	IF
F-actin	A30107	Invitrogen	1:1,000	IF
PDGFRα	31645	Cell Signaling	1:500	IF
F4/80	MF48000	Invitrogen	1:500	IF
p120	610133	BD Biosciences	1:100	IF
CD9	ab92726	Abcam	1:500	IF
CD63	NBP2_32830	Novus	1:200	IF
LAMP1	1D48	DHSB	1:100	IF
RAB7	9367	Cell Signaling	1:200	IF
RAB27A	A1934	ABclonal	1:200	IF

IF, immunofluorescence; WB, Western blot.

of KO strategies is shown in Figure 2*A*. Of 49 clones, 1 contained deletion of the targeted sequence. Loss of cortactin gene and protein expression was confirmed by PCR and Western blot, respectively.

Quantitative Real-time PCR

Total RNA was extracted from cortactin WT and KO Meta4 organoids using TRIzol (Thermo Fisher Scientific) with 0.2% glycogen. cDNA synthesis from the extracted total RNA was performed using iScript Reverse Transcriptase Supermix (Bio-Rad). qPCR was performed using SsoAdvanced Universal SYBR Green Supermix (Bio-Rad) and CFX96 Real-Time PCR Detection System (Bio-Rad) under manufacturer's protocol. Relative gene expression was quantified according to $2^{-\Delta\Delta Ct}$ method, and gene level of TATA-binding protein (*Tbp*) was used for normalization. Primer sequences are listed in Table 2.

Western blot Analysis

Protein extraction was done using M-PER lysis buffer (Thermo Fisher Scientific) with protease and phosphatase inhibitors. Protein concentration was checked using a Pierce BCA Protein Concentration assay (Thermo Fisher Scientific). Samples were diluted in lysis buffer and 2× Laemmli Sample Buffer (Bio-Rad) and boiled at 95 °C for 5 minutes before 20 μg of sample was loaded onto a 4% to 20% Mini-

Table 2. Primer List

Gene	Forward (5′-3′)	Reverse (5′-3′)
Cttn	TAGGCATGAGAGTACTACATATT	AATGAAGATGGTTAGGGTCCA
Cd9	CTGTGGCATAGCTGGTCCTTTG	AGACCTCACTGATGGCTTCAGG
Cd63	GGAATCCACTATCCATACCCAGG	CTCTTCACCAGACAGCAGGAGA
Cd81	CCACCATACTGAGGAACAGCCT	CCACCATACTGAGGAACAGCCT
Alix	GGACTCCATCCAATGACCTGTAC	CGGCTTACACAGAAGTGCGATG
Tsg101	GGTTATCCTGGCTGTCCTTACC	GCACGGATAGTGTCCTCACTGA
Lamp1	CCAGGCTTTCAAGGTGGACAGT	GGTAGGCAATGAGGACGATGAG
Rab7	GAGCGGACTTTCTGACCAAGGA	CAATCTGCACCTCTGTAGAAGGC
Rab27a	GAGCAAAGTTTCCTCAATGTCCG	CTTTCACTGCCCTCTGGTCTTC
Ki-67	ATCATTGACCGCTCCTTTAGGT	GCTCGCCTTGATGGTTCCT
Pcna	GCGTGAACCTCACCAGTATGT	TCTTCGGCCCTTAGTGTAATGAT
Cd44v9	GGAGATCAGGATGACTCCTTCT	AGTCCTTGGATGAGTCTCGATC
Aqp5	TTATCCATTGGCTTGTCGGTCA	GTCCTCCTCTGGCTCATATGTG
He4	TGCCTGCCTGTCGCCTCTG	TGTCCGCACAGTCCTTGTCCA
Tff2	TGCTTTGATCTTGGATGCTG	GGAAAAGCAGCAGTTTCGAC
Tff3	TTGCTGGGTCCTCTGGGATAG	TACACTGCTCCGATGTGACAG
Villin	TCAAAGGCTCTCTCAACATCAC	GGTGCTGGAAGGAACAGG
Trop2	CTGACCTAGACTCCGAGCTG	CGGCCCATGAACAGTGACTC
Cldn7	CTGCCTTGGTAGCATGTTCCTG	CCAGCCGATAAAGATGGCAGGT
Coro1b	CAGCCCGAAATGTGCTTCTCAG	GCAAAAGAGGCTGCCATTGTGG
Actg2	CATTGCTGACAGGATGCAGAAGG	AGCCGCCAATCCAGACTGAGTA
Myo5a	TTGTGGAGCAGGCGAAGGAGAT	GCCTCTCATCATTCAGGTCAAGC
Cd40	ACCAGCAAGGATTGCGAGGCAT	GGATGACAGACGGTATCAGTGG
Atg5	CTTGCATCAAGTTCAGCTCTTCC	AAGTGAGCCTCAACCGCATCCT
Lamp2	GAGCAGGTGCTTTCTGTGTCTAG	GCCTGAAAGACCAGCACCAACT
Lc3b	CCATTCACCAGGAGGAAGAAGG	GCCTGAAAGACCAGCACCAACT
Flot1	CACTCGTTAGGAAAGGCTCGCA	CACTGTGCAGATACCTTCTCCTG
Rab27b	CCTCACCAGTCAACAGAGCTTC	GCCGTTCATTGACTTCCCTTTGG
Rab11a	CAAGAAGCATCCAGGTTGATGGG	AAGGCACCTACTGCTCCACGAT
Rab35	GGTGGTAGAGACAGAAGATGCC	TCTTTGCTCGCAGAACCAGCTC
Tbp	CAAACCCAGAATTGTTCTCCTT	ATGTGGTCTTCCTGAATCCCT
Espn	TCGTTCCTCGTCTTCTACTGGC	TCGTTCCTCGTCTTCTACTGGC
Ezr	TCGTTCCTCGTCTTCTACTGGC	CGGAGCATCTGCTCCTTTTCTC
Stx3	CAACAGATGAGGAGCTGGAAGAG	ATGCTGCTCTCCAGCCTTACGA
Itga2	TACAGACGTGCTCCTGGTAGGT	CCGAGCATTTCCAGTGCCTTCT
Cdh1	GGTCATCAGTGTGCTCACCTCT	GCTGTTGTGCTCAAGCCTTCAC
Epcam	GAGTCCGAAGAACCGACAAGGA	GATGTGAACGCCTCTTGAAGCG

Protean precast gel (Bio-Rad). Transfer was performed at 100 V for 1 hour at 4 °C. The membrane was blocked with 5% non-fat milk in Tris-buffered saline with Tween-20 (TBST) and primary incubation with corresponding antibodies overnight. Membranes were washed 3 times with TBST and incubated with HRP-conjugated secondary antibodies for 1 hour at RT. Membrane was treated with Super Signal West Femto (Thermo Fisher Scientific) before being imaged with Amsheram Imager 680 (GE Healthcare). Antibodies used are listed in Table 1.

Transmission Electron Microscopy

For TEM preparation, Meta4 organoids were washed in 0.1 M cacodylate buffer and fixed in 2% PFA, 2.5% glutaraldehyde, and 0.1 M cacodylate buffer at RT for 1 hour, then overnight at 4 °C. Organoids were washed with 0.1 M cacodylate buffer at RT for 10 minutes, treated with 1% osmium tetroxide in 0.1 M cacodylate buffer for 1 hour, and washed with 0.1 M cacodylate buffer for 10 minutes, then with distilled water for 10 minutes at RT. Samples were treated with 2% uranyl acetate for 30 minutes and subjected to ethanol dehydrations from 30% and 100%, with a final incubation in 100% ethanol and propylene oxide (PO) for 5 min followed by two washes of pure PO. The organoids were infiltrated with Epon 812 resin (Electron Microscopy Sciences) and PO (1:3) for 30 minutes at RT, and then infiltrated with Epon 812 resin and PO (1:1) for overnight at RT. The next day, samples went through a resin:PO (3:1) exchange for 3 to 4 hours and were then incubated with pure epoxy resin overnight. Organoids were incubated in 2 more changes of pure epoxy resin and allowed to polymerize at 60 °C for 48 hours. Ultrathin sections (70- to 80-nm thick) were cut and collected on 300-mesh copper grids. The sections were stained with 2% uranyl acetate and then with Reynold's lead citrate. The organoids were observed using a Philips/FEI T-12 Tecnai T12 electron microscope in 100 kV. Samples were prepared, processed, and imaged by Vanderbilt Cell Imaging Shared Resource (CISR) Core (Vanderbilt University).

Immunocytochemistry

Two-D cultured cells were fixed in 4% PFA for 30 minutes and permeabilized in 0.1% saponin (Sigma-Aldrich) in 3% bovine serum albumin (BSA) for 15 minutes at RT. Cells were incubated with primary antibodies diluted in 0.05% saponin in 3% BSA for 1 hour. Alexa-conjugated secondary antibodies diluted in 3% BSA were incubated for 1 hour, and Hoechst (1:5,000) was added to each well. After 5 minutes of incubation, cells were washed in Dulbecco's phosphate-buffered saline (DPBS, Corning) 3 times and mounted in Prolong Gold Antifade Mountant (Thermo Fischer Scientific).

In Vivo Tumorigenicity Assay

Cortactin WT and KO Meta4 organoids were collected using wide bore tips, maintaining the 3D spherical structures. About 400 to 500 organoid spheres resuspended in 100 μL of ECM gel, 3 days after the split, were subcutaneously implanted into female Nu/J mice at 6 weeks of age (Jackson Laboratory) using a 1-mL syringe with a 19-gauge needle. Cortactin WT organoids were implanted into the left flanks, and KO organoids were implanted into the right flanks of the mice. Engraftment and tumor sizes were measured using a caliper twice a week, and tumor volume was calculated by length (L) $\times$ width (W).[2] The developed engraftments and tumors were collected at 6 and 13 weeks, respectively. To examine the roles of exosomes in the tumorigenicity of dysplastic cells, 10% DMSO and 90% corn oil (Sigma-Aldrich) (vehicle) or 2.5 mg/kg Nexinhib20 dissolved in vehicle was intraperitoneally injected into mice 4 weeks after the Meta4 organoid injection, 3 times a week for 6 weeks. Tumor sizes were measured once a week. The collected tissues were fixed in 4% PFA overnight at 4 °C, embedded in paraffin, and sectioned for histologic examination and immunostaining. The care, maintenance, and treatment of mice used in this study were approved by the Institutional Animal Care and Use Committee of Vanderbilt University.

Air-liquid Interface Culture and Whole Mount Staining

Cortactin WT or KO Meta4 organoids in ECM Gel were dissociated using TrypLE reagent (Gibco), and 30,000 cells/well dissociated cells resuspended in IntestiCult media were plated on top of Transwells (Corning) coated with type I collagen (2.7 mg/cm^2). IntestiCult media supplemented with Y-27632 was added to both top and bottom of well. Three days after plating, the media on the Transwell was removed to expose dysplastic cells to air, and only the media at the bottom of wells were maintained. The ALI culture was maintained for 1 month by replacement of 300 μL of IntestiCult media supplemented with Y-27632 every other day, and conditioned media was collected and frozen at -80 °C for further exosome isolation experiment. Fluid build-up from the cell layer was removed every day, excluding weekend days. The same protocol was applied to Meta4 ALI cultures to treat with either DMSO or 5 μM Nexinhib20 for 2 weeks. To stain the ALI-cultured samples, filters excised from the Transwells were fixed in 4% PFA for 30 minutes at RT, followed by 3 washes in PBS. Blocking was performed with 0.3% Triton X-100 in 10% normal donkey serum. Primary antibodies were diluted in Antibody Diluent (Dako) and applied to each well for overnight incubation at 4 °C. After 3 washes in PBS, samples were incubated in secondary antibodies in Antibody Diluent (Dako) for 4 hours at RT and mounted in Prolong Gold Antifade Mountant containing Hoechst (1:10,000). Images were captured under ZEISS LSM710 confocal microscopy.

EV Isolation and quantification

Frozen conditioned media from the ALI cultures was thawed at 4 °C; 3 independent samples per group were combined in a tube and centrifuged at 300 $\times g$ for 10 minutes and 2,000 $\times g$ for 30 minutes to eliminate cells and cell debris. The supernatants were serially centrifuged at 10,000 $\times g$ for 30 minutes (10,249 rpm in MLA-55 rotor,

Beckman Coulter) and 100,000 × g for 18 hours (32,410 rpm in MLA-55 rotor). The pellets from 10,000 × g and 100,000 × g centrifugation were resuspended in PBS, re-centrifuged at 10,000 × g for 30 minutes and 100,000 × g for 18 hours, respectively, using TLA-110 rotor (13,499 rpm and 42,687 rpm, respectively, Beckman Coulter), and resuspended in PBS. Resuspended large and small EVs (pellets from 10,000 × g and 100,000 × g centrifugation, respectively) were used for nanoparticle tracking analysis (NTA) or Western blot analysis. NTA was performed by analyzing the concentration and size distribution of EV samples using ZetaView (Particle Metrix). EVs were diluted in PBS and measured in a scattered mode by a 488-nm laser. Camera sensitivity was set at 80 for both large and small EVs. Camera frame rate was 7.5 and 30 for large and small Evs, respectively. Large Evs were measured at 85 and small Evs at 70 of the camera shutter level.

Statistical Analysis

To analyze growth behaviors of organoids, 3D cultures in ECM gel containing at least 20 organoid spheres were used in each experiment. Outward or inward budding was quantified based on the phase contrast images obtained from EVOS M7000. Average gaps between epithelial cells and microenvironmental cells were quantified according to the strategy shown in Figure 7*D*, using ImageJ (National Institutes of Health). The area of the closest stromal cells to the epithelial cell region was divided by the perimeter of the epithelial cell region. The number of secreted exosomes in TEM images was normalized to the lateral membrane length of the secreting cells using ImageJ. All authors had access to the study data and had reviewed and approved the final manuscript. All experiments, not otherwise indicated, were repeated at least 3 times, and data on graph were presented as mean ± standard deviation (SD). Data were analyzed by 2-tailed Student's t-test using GraphPad Prism 9 (GraphPad Software, Inc), as described in each figure legend (*$P < .05$; **$P < .01$; and ***$P < .001$).

References

1. Smyth EC, Nilsson M, Grabsch HI, et al. Gastric cancer. Lancet 2020;396:635–648.
2. Sung JK. Diagnosis and management of gastric dysplasia. Korean J Intern Med 2016;31:201–209.
3. Shin SH, Jung DH, Kim JH, et al. Helicobacter pylori eradication prevents metachronous gastric neoplasms after endoscopic resection of gastric dysplasia. PLoS One 2015;10:e0143257.
4. Moon HS, Yun GY, Kim JS, et al. Risk factors for metachronous gastric carcinoma development after endoscopic resection of gastric dysplasia: Retrospective, single-center study. World J Gastroenterol 2017; 23:4407–4415.
5. Min J, Zhang C, Bliton RJ, et al. Dysplastic stem cell plasticity functions as a driving force for neoplastic transformation of precancerous gastric mucosa. Gastroenterology 2022;163:875–890.
6. Min J, Vega PN, Engevik AC, et al. Heterogeneity and dynamics of active Kras-induced dysplastic lineages from mouse corpus stomach. Nat Commun 2019;10:5549.
7. Choi E, Hendley AM, Bailey JM, et al. Expression of activated Ras in gastric chief cells of mice leads to the full spectrum of metaplastic lineage transitions. Gastroenterology 2016;150:918–930.e13.
8. Won Y, Choi E. Mouse models of Kras activation in gastric cancer. Exp Mol Med 2022;54:1793–1798.
9. Douchi D, Yamamura A, Matsuo J, et al. induction of gastric cancer by successive oncogenic activation in the corpus. Gastroenterology 2021;161:1907–1923.e26.
10. Kirkbride KC, Sung BH, Sinha S, Weaver AM. Cortactin: a multifunctional regulator of cellular invasiveness. Cell Adh Migr 2011;5:187–198.
11. Weaver AM, Heuser JE, Karginov AV, et al. Interaction of cortactin and N-WASp with Arp2/3 complex. Curr Biol 2002;12:1270–1278.
12. Luo ML, Shen XM, Zhang Y, et al. Amplification and overexpression of CTTN (EMS1) contribute to the metastasis of esophageal squamous cell carcinoma by promoting cell migration and anoikis resistance. Cancer Res 2006;66(24):11690–11699.
13. Wang X, Cao W, Mo M, Wang W, Wu H, Wang J. VEGF and cortactin expression are independent predictors of tumor recurrence following curative resection of gastric cancer. J Surg Oncol 2010;102:325–330.
14. Cai JH, Zhao R, Zhu JW, et al. Expression of cortactin correlates with a poor prognosis in patients with stages II-III colorectal adenocarcinoma. J Gastrointest Surg 2010;14:1248–1257.
15. Hui R, Campbell DH, Lee CS, et al. EMS1 amplification can occur independently of CCND1 or INT-2 amplification at 11q13 and may identify different phenotypes in primary breast cancer. Oncogene 1997;15:1617–1623.
16. Weaver AM, Karginov AV, Kinley AW, et al. Cortactin promotes and stabilizes Arp2/3-induced actin filament network formation. Curr Biol 2001;11:370–374.
17. MacGrath SM, Koleske AJ. Cortactin in cell migration and cancer at a glance. J Cell Sci 2012; 125:1621–1626.
18. Clark ES, Whigham AS, Yarbrough WG, Weaver AM. Cortactin is an essential regulator of matrix metalloproteinase secretion and extracellular matrix degradation in invadopodia. Cancer Res 2007;67:4227–4235.
19. Sung BH, Zhu X, Kaverina I, Weaver AM. Cortactin controls cell motility and lamellipodial dynamics by regulating ECM secretion. Curr Biol 2011;21:1460–1469.
20. Maas SLN, Breakefield XO, Weaver AM. Extracellular vesicles: unique intercellular delivery vehicles. Trends Cell Biol 2017;27:172–188.
21. Hoshino D, Kirkbride KC, Costello K, et al. Exosome secretion is enhanced by invadopodia and drives invasive behavior. Cell Rep 2013;5:1159–1168.
22. Sung BH, Ketova T, Hoshino D, et al. Directional cell movement through tissues is controlled by exosome secretion. Nat Commun 2015;6:7164.
23. Sung BH, Weaver AM. Exosome secretion promotes chemotaxis of cancer cells. Cell Adh Migr 2017;11:187–195.

24. Sato S, Weaver AM. Extracellular vesicles: important collaborators in cancer progression. Essays Biochem 2018;62:149–163.
25. Weed SA, Karginov AV, Schafer DA, et al. Cortactin localization to sites of actin assembly in lamellipodia requires interactions with F-actin and the Arp2/3 complex. J Cell Biol 2000;151:29–40.
26. Bryce NS, Clark ES, Leysath JL, et al. Cortactin promotes cell motility by enhancing lamellipodial persistence. Curr Biol 2005;15:1276–1285.
27. Radhakrishnan VM, Kojs P, Young G, et al. pTyr421 cortactin is overexpressed in colon cancer and is dephosphorylated by curcumin: involvement of non-receptor type 1 protein tyrosine phosphatase (PTPN1). PLoS One 2014;9:e85796.
28. El Sayegh TY, Arora PD, Laschinger CA, et al. Cortactin associates with N-cadherin adhesions and mediates intercellular adhesion strengthening in fibroblasts. J Cell Sci 2004;117:5117–5131.
29. Lee SH, Contreras Panta EW, Gibbs D, et al. Apposition of fibroblasts with metaplastic gastric cells promotes dysplastic transition. Gastroenterology 2023;165:374–390.
30. Li I, Nabet BY. Exosomes in the tumor microenvironment as mediators of cancer therapy resistance. Mol Cancer 2019;18:32.
31. Sinha S, Hoshino D, Hong NH, et al. Cortactin promotes exosome secretion by controlling branched actin dynamics. J Cell Biol 2016;214:197–213.
32. Zhang Y, Liu Y, Liu H, Tang WH. Exosomes: biogenesis, biologic function and clinical potential. Cell Biosci 2019;9:19.
33. Hessvik NP, Llorente A. Current knowledge on exosome biogenesis and release. Cell Mol Life Sci 2018; 75:193–208.
34. Xu M, Ji J, Jin D, et al. The biogenesis and secretion of exosomes and multivesicular bodies (MVBs): intercellular shuttles and implications in human diseases. Genes Dis 2023;10:1894–1907.
35. Lewis V, Green SA, Marsh M, et al. Glycoproteins of the lysosomal membrane. J Cell Biol 1985;100:1839–1847.
36. Ostrowski M, Carmo NB, Krumeich S, et al. Rab27a and Rab27b control different steps of the exosome secretion pathway. Nat Cell Biol 2010;12:19–30, sup pp 1–13.
37. Raposo G, Stoorvogel W. Extracellular vesicles: exosomes, microvesicles, and friends. J Cell Biol 2013; 200:373–383.
38. Lotvall J, Hill AF, Hochberg F, et al. Minimal experimental requirements for definition of extracellular vesicles and their functions: a position statement from the International Society for Extracellular Vesicles. J Extracell Vesicles 2014;3:26913.
39. Johnson JL, Ramadass M, He J, et al. Identification of neutrophil exocytosis inhibitors (Nexinhibs), small molecule inhibitors of neutrophil exocytosis and inflammation: druggability of the small GTPase Rab27a. J Biol Chem 2016;291:25965–25982.
40. Hanahan D, Weinberg RA. Hallmarks of cancer: the next generation. Cell 2011;144:646–674.
41. Buday L, Downward J. Roles of cortactin in tumor pathogenesis. Biochim Biophys Acta 2007;1775: 263–273.
42. Velazquez-Avila M, Balandran JC, Ramirez-Ramirez D, et al. High cortactin expression in B-cell acute lymphoblastic leukemia is associated with increased transendothelial migration and bone marrow relapse. Leukemia 2019;33:1337–1348.
43. Lang L, Hou Y, Chen Y, et al. ATM-mediated phosphorylation of cortactin involved in actin polymerization promotes breast cancer cells migration and invasion. Cell Physiol Biochem 2018;51:2972–2988.
44. Zuo Q, Wu W, Li X, et al. HDAC6 and SIRT2 promote bladder cancer cell migration and invasion by targeting cortactin. Oncol Rep 2012;27:819–824.
45. Ji J, Feng X, Shi M, et al. Rac1 is correlated with aggressiveness and a potential therapeutic target for gastric cancer. Int J Oncol 2015;46:1343–1353.
46. Kurayoshi M, Oue N, Yamamoto H, et al. Expression of Wnt-5a is correlated with aggressiveness of gastric cancer by stimulating cell migration and invasion. Cancer Res 2006;66:10439–10448.
47. Ming SC, Bajtai A, Correa P, et al. Gastric dysplasia. Significance and pathologic criteria. Cancer 1984;54:1794–1801.
48. Anderson NM, Simon MC. The tumor microenvironment. Curr Biol 2020;30:R921–R925.
49. Maia J, Caja S, Strano Moraes MC, et al. Exosome-based cell-cell communication in the tumor microenvironment. Front Cell Dev Biol 2018;6:18.
50. Brucher BL, Jamall IS. Cell-cell communication in the tumor microenvironment, carcinogenesis, and anticancer treatment. Cell Physiol Biochem 2014;34:213–243.
51. Ungefroren H, Sebens S, Seidl D, et al. Interaction of tumor cells with the microenvironment. Cell Commun Signal 2011;9:18.
52. Kahlert C, Kalluri R. Exosomes in tumor microenvironment influence cancer progression and metastasis. J Mol Med (Berl) 2013;91:431–437.

Received February 14, 2024. Accepted February 25, 2025.

Correspondence
Address correspondence to: Eunyoung Choi, PhD, 2213 Garland Ave, Medical Research Building IV, Room 10445, Nashville, Tennesse 37232. e-mail: eunyoung.choi@vumc.org; tel: (615) 322-0775.

CRediT Authorship Contributions

Alexis A. Guenther (Conceptualization: Equal; Data curation: Lead; Formal analysis: Lead; Investigation: Lead; Methodology: Lead; Validation: Lead; Visualization: Lead; Writing – original draft: Lead; Writing – review & editing: Lead)

Suyeon Ahn, PhD (Conceptualization: Equal; Data curation: Equal; Formal analysis: Lead; Investigation: Lead; Methodology: Equal; Validation: Lead; Visualization: Lead; Writing – original draft: Lead; Writing – review & editing: Lead)

Jimin Min, PhD (Conceptualization: Lead; Data curation: Lead; Formal analysis: Lead; Investigation: Lead; Methodology: Lead; Validation: Lead; Visualization: Lead; Writing – original draft: Lead; Writing – review & editing: Lead)

Changqing Zhang (Methodology: Supporting)

Hyuk-Joon Lee, MD, PhD (Resources: Supporting)

Han-Kwang Yang, MD, PhD (Resources: Supporting)

Bong Hwan Sung, PhD (Data curation: Equal; Formal analysis: Equal; Investigation: Equal; Methodology: Equal; Validation: Equal; Visualization: Equal; Writing – review & editing: Supporting)

Alissa M. Weaver, PhD (Funding acquisition: Lead; Methodology: Supporting; Supervision: Supporting; Writing – review & editing: Supporting)

Eunyoung Choi, PhD (Conceptualization: Lead; Funding acquisition: Lead; Methodology: Supporting; Supervision: Lead; Writing – original draft: Lead; Writing – review & editing: Lead)

Conflicts of interest
The authors disclose no conflicts.

Funding
This work was supported by National Institutes of Health (NIH) grants R37 CA244970 and R01 CA272687 and VICC GI SPORE (P50 CA236733), the AGA Research Foundation's AGA-R. Robert & Sally Funderburg Research Award in Gastric Cancer (AGA2022-32-01), and the Gastric Cancer Foundation (to Eunyoung Choi), R01CA249684 and R01CA206458 (to Alissa M. Weaver), and R50CA283661 (to Bong Hwan Sung). Core Services performed through Vanderbilt University Medical Center's Digestive Disease Research Center (P30 DK058404) and Vanderbilt-Ingram Cancer Center (P30 CA068485) with imaging in the Vanderbilt Digital Histology Shared supported by a VA Shared Instrumentation grant (1IS1BX003097). The specimen preparation and imaging were performed in part through the use of the Vanderbilt Translational Pathology Shared Resource (supported by NCI/NIH Cancer Center Support Grant P30CA068485) and the Vanderbilt Cell Imaging Shared Resource (supported by NIH grants CA68485, DK20593, DK58404, DK59637, and EY08126).

Data Availability
All data are available in the main text.